Cocaine addiction-like behaviors are associated with long-term changes in gene regulation, energy metabolism, and GABAergic inhibition within the amygdala

Jessica L. Zhou[1,2], Giordano de Guglielmo[3], Aaron J. Ho[2], Marsida Kallupi[3], Narayan Pokhrel[3], Hai-Ri Li[4], Apurva S. Chitre[3], Daniel Munro[3,5], Pejman Mohammadi[5,6,7,8], Lieselot LG Carrette[3], Olivier George[3], Abraham A. Palmer[3,9], Graham McVicker*[1,2], Francesca Telese*[3,4]

[1]Bioinformatics and Systems Biology Program, University of California San Diego, La Jolla, CA, 92093, USA
[2]Integrative Biology Laboratory, Salk Institute for Biological Studies, La Jolla, CA 92037
[3]Department of Psychiatry, University of California, San Diego, La Jolla, CA, 92092, USA
[4]Department of Medicine, University of California San Diego, La Jolla, CA 92093, USA
[5]Department of Integrative Structural and Computational Biology, The Scripps Research Institute, La Jolla, CA, 92037, USA
[6]Center for Immunity and Immunotherapies, Seattle Children's Research Institute, Seattle, WA, 98145, USA
[7]Department of Pediatrics, University of Washington School of Medicine, Seattle, WA, 98195, USA
[8]Department of Genome Sciences, University of Washington, Seattle, WA, 98195, USA
[9]Institute for Genomic Medicine, University of California San Diego, La Jolla, CA 92093, USA

*Correspondence:
Francesca Telese (ftelese@health.ucsd.edu)
Graham McVicker (gmcvicker@salk.edu)

Abstract

The amygdala processes positive and negative valence and contributes to the development of addiction, but the underlying cell type-specific gene regulatory programs are unknown. We generated an atlas of single nucleus gene expression and chromatin accessibility in the amygdala of outbred rats with low and high cocaine addiction-like behaviors following prolonged abstinence. Between rats with different addiction indexes, we identified thousands of cell type-specific differentially expressed genes enriched for energy metabolism-related pathways that are known to affect synaptic transmission and action potentials. Rats with high addiction-like behaviors showed enhanced GABAergic transmission in the amygdala, which, along with relapse-like behaviors, were reversed by inhibition of Glyoxalase 1, which metabolizes the $GABA_A$ receptor agonist methylglyoxal. Finally, we identified thousands of cell type-specific chromatin accessible sites and transcription factor (TF) motifs where accessibility was associated with addiction index, most notably at motifs for pioneer TFs in the Fox, Sox, helix-loop-helix, and AP1 families.

Introduction

The amygdala is a key brain region involved in regulating a wide range of behaviors, including those related to emotions, motivation and memory[1]. In response to rewarding or aversive environmental stimuli, the amygdala allows organisms to engage in subsequent valence-specific behaviors by determining the value of different stimuli and guiding decision-making based on potential outcomes[1]. The amygdala is implicated in numerous neuropsychiatric disorders including addiction[2–4]. Repeated drug use leads to a heightened sense of pleasure, which engages the amygdala to form drug-associated memories and reinforces drug-seeking behavior, as the individual is motivated to seek out and use the drug again in order to experience the rewarding effects[5]. In addition, during withdrawal from addictive drugs, the amygdala mediates negative emotional states, such as anxiety, fear, and irritability[5]. Avoidance of these aversive emotions enhances the incentive value of the drug, leading to sustained drug-seeking behaviors and relapse[6–8]. Because prevention of relapse is the cornerstone of effective treatments for addiction, it is important to understand the amygdala's role in addiction and relapse.

The amygdala is composed of multiple discrete and interconnected subregions, each characterized by highly specialized neuronal populations distinguishable by their morphology and electrophysiological properties[9]. The major subdivisions include the basolateral amygdala (BLA), composed of excitatory glutamatergic neurons and GABAergic inhibitory interneurons, and the central amygdala (CeA), composed of GABAergic neurons[10–12]. While the behavioral function and connectivity of individual subregions of the amygdala have recently been established[1], the mechanisms by which distinct subpopulations of neuronal and non-neuronal cells contribute to its function remains unclear.

Single-cell genomics is a powerful new approach for determining the cellular function and diversity of complex tissues like the amygdala. Single-cell RNA-sequencing (scRNA-seq), which profiles gene expression in individual cells, has identified and cataloged diverse cell types in human, mouse, and non-human primate brains[13–19]. In addition, single-cell assays for transposase-accessible chromatin (scATAC-seq), which profile chromatin accessibility at single cell resolution, have identified regulatory DNA sequences in the rodent and human brain[13,20–26]. Regulatory elements identified by scATAC-seq include promoters and enhancers, which confer cell type-specificity to gene expression by recruiting sequence-specific transcription factors (TFs)[27–30].

Single cell assays have the potential to reveal, at a molecular level, how specialized amygdalar cell populations are involved in addiction. For example, given that most genetic variants associated with complex human diseases like addiction are located in noncoding regions of the genome[31], snATAC-seq could uncover genetically determined, cell-type specific differences and facilitate functional interpretation of genetic variants[32]. Thus far, however, the application of single-cell assays to the study of addiction-like behaviors in rodents has been limited. Single nucleus RNA-seq (snRNA-seq) has been applied to characterize cellular diversity in brain regions involved in the reward system[33–36], and has been used to analyze transcriptional changes induced by cocaine and morphine[37,38]. However, these prior studies used isogenic rodents, which means that genetically-mediated differences in susceptibility to addiction-like behaviors were not examined. Furthermore, these studies performed experiments following acute, experimenter-administration of drug treatments, which means that they reflect the acute effects of involuntary drug use rather than molecular differences associated with the development of long-lasting addictive-like behaviors. For these reasons, the results from prior single nucleus studies have significant limitations.

To address this knowledge gap, we performed snRNA-seq and snATAC-seq using amygdala tissue from outbred rats obtained from a large genetic study of cocaine addiction-related traits[39]. These rats are subjected to prolonged abstinence from voluntary cocaine intake in a well-validated model of extended access to drug intravenous self-administration (IVSA)[6,39–41]. IVSA is associated with neurochemical changes in key brain regions, which are thought to be similar to those observed in humans with cocaine use disorder[42]. This study used outbred heterogeneous stock (HS) rats because they have high levels of genetic variation and rich phenotypic diversity[43–46]. By analyzing differences in gene expression and chromatin accessibility in rats with high and low addiction indexes (AI), we identified genes and transcriptional regulators associated with cocaine addiction-like behaviors, including those implicated in energy metabolism and neurotransmitter pathways. Furthermore, using genetic predictions of gene expression, we found that genetic differences contribute to the gene expression differences between high and low AI rats. Finally, we performed pharmacological manipulation of $GABA_A$ receptor signaling in amygdalar tissue slices and in rats to validate insights gained from the transcriptomic data.

Results

Behavioral characterization of HS rats exhibiting low or high cocaine addiction-like traits

To investigate how chronic cocaine use influences cellular states associated with addiction-like behaviors, we performed snRNA-seq and snATAC-seq on amygdala tissues from HS rats subjected to protracted abstinence (4 weeks) following extended access to cocaine IVSA [39,47–50] (Fig. 1a). The animals were trained to self-administer cocaine via lever press (0.5 mg/kg/infusion) in operant chambers in short access (ShA, 2h/day, 5 days per week) and long access (LgA, 6h/day, 5 days/week) sessions. We measured the number of cocaine infusions, or lever presses, during each session of the behavioral protocol to quantify escalation of intake, motivation, and compulsive-like behavior. Specifically, we measured escalation as the increase in the mean number of cocaine rewards during each of the LgA sessions compared to the first day of the LgA phase; we measured motivation as the mean number of cocaine rewards over the ShA and LgA sessions under a progressive ratio (PR) schedule of reinforcement, which is when the number of lever presses required to obtain a cocaine infusion was progressively increased; and we measured compulsive-like behavior as drug taking despite adverse consequences, by pairing 30% of lever presses with an electric foot shock (Fig. 1b). Based on individual behavioral measures for each rat (Fig. 1c), we calculated an addiction index (AI)[39] as the average of the normalized values (z-scores) of the three behavioral measures. Prior work has demonstrated that AI measures vulnerability (high AI) or resilience (low AI) to developing cocaine addiction-like behaviors[39,51–53].

We classified rats into high and low AI groups (Fig. 1d). Both high and low AI rats acquired fewer cocaine rewards in the ShA compared to the LgA sessions of the IVSA protocol (Fig. 1e, two-way repeated measures ANOVA, addiction index × phase interaction $p<0.0001$, $F_{23,1012}=8.523$). There was no difference between groups in cocaine rewards during ShA sessions. However, we observed a contrasting pattern in escalation during LgA sessions. During LgA sessions, rats with high AI exhibited a progressive escalation of drug intake compared to rats with low AI as evidenced by their increased number of cocaine infusions over the course of this phase of the IVSA protocol (two-way repeated measures ANOVA interaction time x group $F_{13,572}=4.175$, $p < 0.0001$, Fig. 1e). In contrast, low AI rats did not show escalation during the LgA sessions (Fig. 1e).

During PR sessions, motivation for cocaine increased in the high AI rats but not in low AI rats when comparing ShA versus LgA (Fig. 1f, mixed effect model, addiction index × phase interaction, $p=0.0049$, $F_{1,41}=8.83$; Bonferroni corrected $p=0.0001$, post hoc comparisons). Finally, high AI rats showed increased responses despite adverse consequences compared to low AI rats, as demonstrated by the higher number of cocaine infusions when the reward was paired with an electric foot shock (Fig. 1g, $p<0.001$, unpaired Student's t-test, $t_{44}=3.936$), which may reflect compulsive-like drug use. These results show that we can capture multiple

behavioral aspects that are relevant to cocaine use disorders by using this model of extended access to cocaine IVSA in outbred rats.

snRNA-seq and snATAC-seq defines distinct populations of cell types in the amygdala

The amygdala is thought to contribute to the development of addiction through its regulation of drug-seeking behavior, which, in rats, progressively increases after withdrawal from drug IVSA[6,54]. To identify neuroadaptations that persist in the amygdala after chronic drug exposure during the withdrawal stage, we collected amygdalae after 4 weeks of abstinence from cocaine IVSA (Fig. 1a). We purified nuclei and measured the gene expression and chromatin accessibility profiles of individual nuclei by performing snRNA-seq and snATAC-seq with the 10X Genomics Chromium workflow. We performed these experiments on high and low AI rats, as well as naive rats never exposed to cocaine. For snRNA-seq, we used 19 rats including 6 with high AI, 6 with low AI, and 7 naive rats (Supplementary Data 1). For snATAC-seq we used 12 rats including 4 with high AI, 4 with low AI, and 4 naive rats (Supplementary Data 2).

After filtering low quality nuclei and potential doublets based on quality metrics, we obtained a combined total of 163,003 and 81,912 high quality nuclei from the snRNA-seq and snATAC-seq samples, respectively (Fig. S1-6, Supplementary Data 3-4). Across the snRNA-seq samples, the mean reads per cell varied from 11,967 to 50,343 and the median number of detected genes ranged from 1,293 to 2,855. Across the 12 snATAC-seq samples, the median number of high-quality fragments per nucleus ranged from 7,111 to 22,018. Across samples, we observed means of 8579 and 6826 nuclei per rat in the snRNA-seq and snATAC-seq datasets, respectively (Fig. S7). The above metrics are consistent with previously published single-nucleus sequencing studies of the amygdala[33,55]. Using these data, we performed normalization, integration across rats, dimensionality reduction and clustering using Seurat[56] (for snRNA-seq) and Signac[57] (for snATAC-seq). In total, we identified 49 cell type clusters in the integrated snRNA-seq dataset and 41 cell type clusters in the integrated snATAC-seq dataset (Fig. S8). Visualization of the integrated data indicated that the clustering is not influenced by batch effects such as sequencing library, percentage of mitochondrial DNA, or individual rats[58] (Fig. S9).

We annotated the snRNA-seq clusters based on the expression of established cell type-specific marker genes[59–63] (Fig. 2a-b). The major cell types included excitatory neurons (denoted by expression of *Slc17a7)*, inhibitory GABAergic neurons (*Gad1/Gad2)*, astrocytes (*Gja1)*, microglia (*Ctss)*, mature oligodendrocytes (*Cnp)*, oligodendrocyte precursor cells (OPC) (*Pdgfra)*, and endothelial cells (*Cldn5)* (Fig. 2c). To annotate the snATAC-seq clusters, we estimated gene activity from pseudo bulk chromatin accessibility at promoter regions of cell marker genes and used these gene activity scores to impute gene expression in the snATAC-seq samples (Fig. S10). The imputed gene expression clearly delineates the cell clusters into the same major cell types described above demonstrating strong concordance between our snRNA-seq and snATAC-seq data (Fig. 2d). In addition to the major cell types, we also identified seven subtypes of inhibitory neurons based on the expression of known cell marker

genes (Fig. 2e). Cell type proportions appeared to be consistent across samples (Fig. S11-12). We also sub-clustered the excitatory neurons and identified 18 distinct clusters (Fig. S13), with top markers including known subpopulation markers such as *Cdh13, Nr4a2, Bdnf*[64].

The total number of nuclei we obtained for each cell type varied substantially (Fig. 2f). As expected, excitatory and inhibitory neurons are the most common major cell types. The snRNA-seq dataset contains 52,579 (~32.3%) nuclei from inhibitory neurons and 23,943 (~14.7%) nuclei from excitatory neurons (Table S1). The snATAC-seq dataset contains 18,208 (~22.2%) nuclei from inhibitory neurons and 20,169 (~24.6%) nuclei from excitatory neurons (Table S1). Endothelial cells and some subtypes of inhibitory and excitatory neurons have small numbers of nuclei in the dataset, so for most downstream analyses we focused on the six most common major cell types (Fig. 2a-b).

To determine how the cell types we identified in the whole amygdala correspond to cell types within spatially defined amygdalar subregions, we generated snRNA-seq data from the CeA and BLA (Fig. S14). We found that cell clusters from the CeA and BLA were distinct from one another, but these regions collectively contained most cell types also identified in the whole amygdala (Fig. S14a). Consistent with the known cell type composition of the CeA and BLA[65], the cell clusters from the CeA co-clustered primarily with inhibitory neurons while the cell clusters from the BLA co-clustered with excitatory neurons (Fig. S14b). Glial cell types from the whole amygdala contained cells from both subregions, with the exception of astrocytes, which mostly co-clustered with cells from the CeA but not the BLA, suggesting that astrocytes might play a specific role in BLA-related function (Fig. S14a-b).

In combination, the snRNA-seq and snATAC-seq datasets that we generated are the first single-cell atlas of molecularly defined cell types in the rat amygdala. The inclusion of multiple high AI, low AI, and naive rats make these datasets an important resource for studying gene expression and chromatin accessibility in the amygdala under both normal conditions as well as in the context of cocaine addiction-like behaviors.

Measuring cell type-specific differential gene expression between rats displaying a high versus a low addiction index for cocaine

We used the negative binomial test to identify differentially expressed genes (DEGs) between high and low AI rats in each cell type (Fig. 3a-b, Supplementary Data 5). To control for batch effects or violations in the differential expression model assumptions (for example, unaccounted for overdispersion in the data) that can cause deflated (overly significant) p-values, thereby yielding false signals of differential expression[66,67], we performed the same statistical test after permuting the AI labels of the rats. This permutation simulates a null distribution where there is no association between AI and gene expression. This approach is often used to assess p-value calibration in QTL studies[68,69]. While the results from the unpermuted data are highly enriched for low p-values, the p-values from the permuted data resemble the null expectation. This

indicates that the highly-significant DEGs we identified are not due to poor p-value calibration or batch effects (Fig. S15, Supplementary Data 6).

We grouped DEGs into small (abs($\log_2$FC)<0.1) or large effect size groups (abs($\log_2$FC)≥0.1) and observed that most of the significant DEGs (FDR<10%) have small effect sizes (Fig. S16). In total, we identified 557 unique significant DEGs with large effect sizes in at least one cell type and 8,775 unique significant DEGs with small effect sizes in at least one cell type. The number of significant DEGs between high and low AI rats correlates with the size of the cell type population (Fig. S16), which likely reflects greater power to detect differential expression in common cell types. Most of the large effect DEGs (431, or 75%) are also small-effect DEGs in at least one other cell type, indicating that while there are shared patterns of differential expression across cell types, the effect sizes vary across cell types. We also found that significant DEGs were enriched for gene expression quantitative trait loci (eQTLs), which are genetic variants associated with a gene's expression, in rat brain tissues[70] in almost every cell type tested (Chi-squared test with 1 degree of freedom, p<0.05) (Fig. S17, Table S2). This suggests that heritable differences influence the changes in expression that we observed. Among the most significant DEGs with eQTLs (Supplementary Data 7), we identified genes with previously reported roles in cocaine or other substance use disorders. For example, *Kcnq3* was differentially regulated across neuronal and glial cell types, and this gene encodes a subunit of a potassium channel implicated in the regulation of reward behavior and susceptibility to drug addiction (Fig. 3c)[71–73]. Additionally, *Fkbp5* and *Sgk1*, two transcriptional targets of the glucocorticoid receptor, were differentially regulated specifically in glial cell types, and these genes are associated with reward behavior and drug addiction vulnerability (Fig. 3d-e)[74–76]. These results suggest that genetic differences contribute to the gene expression differences between rats with high and low AI.

The observed DEGs could reflect pre-existing genetic differences or the differential exposure to cocaine in the high versus low AI groups. To further examine the contribution of genetics to observed differences in gene expression, we leveraged genotypes and gene expression data from a previously published reference population of 339 naive HS rats[70]. This allowed us to predict gene expression based on cis-genetic variation in the absence of cocaine exposure. Specifically, we trained models which predict gene expression from SNP genotypes[77] using whole brain bulk RNA-seq from 339 naive HS rats. We then used these models to predict the expression of genes with at least one cis-acting eQTL (8,997 genes) in each of the rats in our snRNA-seq dataset. We compared the differences in mean predicted expression in the high versus low AI rats to the observed differences in expression for each cell type. Before correlating predicted expression to observed expression, we filtered out genes for which the predictive models had low Pearson r^2, because genes with higher r^2 have more of their variance in expression explained by cis-genetic variation (Table S3). Among our major cell types, the observed and predicted expression differences were significantly correlated (Spearman's ρ, p<0.05) for microglia, oligodendrocytes and inhibitory neurons (Fig. S18, Table S3). We found that increasing the stringency of the r^2 cutoff increased the strength of these correlations (Fig. S18, Table S3). These observations indicate that genetic differences in high versus low AI rats contribute to at least some of the observed differences in expression between

high vs. low AI rats. Cocaine is also likely to contribute to the differences in expression; however, the relative contributions of cocaine and genetics are difficult to quantify due to limitations in the genetic predictions of gene expression.

To identify pathways with altered regulation between high and low AI rats, we performed gene set enrichment analysis (GSEA)[78,79] of KEGG pathways using estimates of differential gene expression ($\log_2$ fold change) for each cell type. We identified significant enrichment of several pathways related to addiction (e.g. amphetamine, nicotine, and morphine addiction), neurotransmission (e.g. synaptic vesicle cycle, GABAergic synapse, glutamatergic synapse, and dopaminergic synapse), energy metabolism (e.g. glycolysis, pyruvate metabolism, and oxidative phosphorylation), and others (Fig. 3f, Supplementary Data 8). Most cell types showed enrichment of genes belonging to the oxidative phosphorylation pathway, which, together with glucose metabolism, is the main energy source for synaptic activity and action potentials[80,81]. Moreover, different subtypes of inhibitory neurons as well as excitatory neurons were enriched for synaptic vesicle cycle and synapse-related pathways. In combination, these observations suggest that addiction-like behaviors are associated with alterations in the metabolic state of amygdalar cell populations, which can directly impact neural network activity within the amygdala by affecting neurotransmission and synaptic pathways.

The development of cocaine addiction-like behaviors is linked to elevated GABAergic transmission in the amygdala

To test the hypothesis that altered metabolic state in amygdalar cells changes neural activity within the amygdala, we focused on GABAergic transmission because alterations of this neurotransmitter system have been previously described in the amygdala in the context of addiction-related phenotypes[2]. Specifically, we measured GABAergic transmission by recording spontaneous inhibitory postsynaptic currents (sIPSCs) in the central amygdala (CeA). CeA slices were collected from a separate cohort of 5 low AI and 5 high AI HS rats that were subjected to prolonged abstinence following the same behavioral protocol described for the snRNA-seq and snATAC-seq experiments (Fig. 4a). As a control, we used CeA slices prepared from 5 age-matched naive HS rats to record baseline GABAergic transmission. There were differences in mean sIPSC frequencies among the groups (one-way ANOVA $F_{2,22}$=6.77, p=0.0051), reflecting a progressive increase in GABAergic transmission from naive to low AI to high AI rats (Fig. 4b, Fig. S19a), without detectable changes in amplitude (Fig. S19b-c). These results are consistent with the hypothesis that the cocaine addiction-like behaviors exhibited by high AI rats alters GABAergic transmission.

To further investigate the link between GABAergic transmission and energy metabolism in the amygdala with cocaine addiction-like behaviors, we measured siPSCs frequency and amplitude before and after application of S-bromobenzylglutathione cyclopentyl diester (pBBG)[82,83]. pBBG is a small molecule inhibitor of glyoxalase 1 (GLO1), the rate limiting enzyme for the metabolism of methylglyoxal (MG), which is a byproduct of glycolysis that acts as a competitive partial agonist of $GABA_A$ receptors[82]. We found that pBBG reduced the sIPSC frequency compared to vehicle for both high and low AI rats (paired t-tests, t_5=11.83, p=7.6e-5 and t_5=5.07, p=3.9e-3,

respectively), but not naive rats (t_5=0.71, p=0.51) (Fig. 4c-f, Fig. S19a). We observed no effect on iPSCs amplitude (Fig. S19b-c). In most situations, changes in frequency of events indicate presynaptic modulation while changes in amplitude of events reflect postsynaptic modulation; however, previous studies have shown that GABA modulates synaptic transmission presynaptically[84,85]. These findings suggest that Glo1 inhibition may alter presynaptic GABA-A receptor function, leading to reduced GABA release at inhibitory terminals and suppression of inhibitory connections within the CeA.

These results led us to hypothesize that GLO1 inhibition would revert behavioral responses after prolonged abstinence from cocaine IVSA. To test this hypothesis, we measured cue-induced reinstatement of cocaine seeking behavior in a separate cohort of 26 low and high AI rats 30 minutes after systemic injection of pBBG or vehicle[86] following 4 weeks of abstinence from cocaine IVSA (Fig. 4g). During this test, rats were subjected to the same operant conditions of cocaine IVSA, but without drug availability. Then, reinstatement was triggered by re-exposure to the cocaine infusion-associated light cue. The two-way repeated measures ANOVA showed a significant interaction between AI and pBBG treatment ($F_{1,24}$=6.609, p<0.05), indicating that pBBG versus vehicle reduced cue-induced reinstatement in high AI rats (p-value<0.05, post hoc comparisons with Bonferroni correction), but not in low AI rats (p>0.05). Overall these results demonstrate that modulating $GABA_A$ transmission via the pharmacological inhibition of GLO1 decreases relapse-like behaviors in animals with high cocaine AI.

Mapping differences in chromatin accessibility associated with cocaine addiction-like behaviors

To identify regions of accessible chromatin from the snATAC-seq data, we used MACS2[87] to call peaks from the aligned reads for each rat and created a union peak set across rats. We examined pseudo bulk chromatin accessibility at the transcription start site (TSS) of selected cell type marker genes and observed cell type-specific patterns of accessibility at the expected marker genes of each cell type (Fig. 5a, Fig. 2c-d), indicating that the chromatin accessibility corresponds well with the transcriptome measurements.

To better understand the regulatory mechanisms involved in cocaine addiction, we analyzed differences in chromatin accessibility between high and low AI rats. We performed negative binomial[88,89] tests to measure cell type-specific differential chromatin accessibility (Supplementary Data 9), and compared the observed p-values to those obtained from permuted data (as we did for our DEG analysis). The p-values of the permuted data resemble the null expectation, confirming that the differential peaks between high and low AI are likely true biological differences rather than artifacts (e.g. batch effects) (Fig. S20, Supplementary Data 10). In total we identified >20,000 peaks across cell types with significant differential accessibility between the high and low AI groups (FDR<10%), however, as with gene expression, most differences were small ($\log_2$FC < 0.1) (Fig. S21). This indicates that differences in addiction-like behaviors between rats are associated with modest regulatory changes at a large number of sites.

The differential peaks can be subdivided into those where accessibility is higher (upregulated) or lower (downregulated) in the high AI rats (Fig. S21). In astrocytes, there were roughly equal numbers of up- and downregulated peaks, but the other cell types showed profound directional biases. Excitatory neurons were the most biased with only two detected downregulated peaks, and over 8000 upregulated peaks in the high AI group. Inhibitory neurons showed the opposite bias with over 4000 downregulated peaks but only ~500 upregulated peaks in the high AI group (Fig. S21). These biases likely reflect differences in the activity of specific TFs that control large transcriptional programs.

To determine whether the differential chromatin accessibility is consistent with the differential gene expression, we tested whether the promoters of DEGs are enriched for differential accessibility. We overlapped the significant differentially accessible chromatin peaks in each cell type with the promoters of significant DEGs and computed a log odds ratio ($\log_2$OR) as a measure of enrichment. Across all of the major cell types, differentially accessible peaks are enriched (FET, $p<0.05$) at the promoters of DEGs compared to non-DEGs (Fig. 5b, Table S4). We also examined chromatin accessibility at promoter regions for genes belonging to the oxidative phosphorylation pathway because genes within this pathway were enriched for gene expression differences between high vs. low AI rats in a majority of cell types. These genes are also significantly enriched for differentially accessible promoter peaks in inhibitory neurons, excitatory neurons and oligodendrocytes (Fig. S22, Table S5). These findings confirm that the observed differences in chromatin accessibility and gene expression are concordant.

The genomic annotations of the significant differential peaks showed that 3.19% of these regions were annotated as promoter or TSS regions (Fig. S23). While this is a small percentage of the peaks, it is consistent with other studies[26]. We then studied the subset of significant differential peaks in each cell type by examining their genomic annotations to determine if they were enriched for promoter/TSS regions compared to the set of all peaks. We observed that differentially accessible peaks were highly enriched in promoter regions, occurring at least four times more frequently than expected given the genomic annotations of all accessible chromatin regions in most of the major cell types (FET, FDR<10%) (Fig. 5c, Table S6). This enrichment may indicate that long-term changes in chromatin associated with addiction-like behaviors are more concentrated at promoters, or that we have greater statistical power to detect changes at promoters, due to larger effect sizes or greater overall chromatin accessibility.

We hypothesized that differences in chromatin accessibility between high and low AI rats are caused by differential TF activity. To test this hypothesis, we analyzed the snATAC-seq data using ChromVar (Supplementary Dataset 11), which identifies TF motifs associated with differential accessibility using sparse single cell data[90]. A large number of motifs have significant differences in accessibility between the high and low AI rats, and since many TFs recognize similar motifs, we grouped them into motif clusters and summarized results across cell types (Fig. 5d).

The motif cluster with the most significant difference in accessibility between high and low AI rats contains motifs for basic helix-loop-helix (bHLH) TFs. This motif cluster has substantially

higher accessibility within the excitatory neurons of high AI rats compared to low AI rats (deviance 3.8, p=1e-280), as well as a modest increase in accessibility in inhibitory neurons (deviance 0.38, p=1e-34) (Fig. 5e-g). The top-ranked motifs in this cluster all harbor the sequence CAGATGG, which is a close match to binding site motifs for multiple neuronal pioneer TFs including those of the bHLH, RFX and FOX families[91,92]. Thus, the widespread increases in chromatin accessibility in excitatory neurons of high AI rats could reflect increased activity of pioneer TFs that recruit chromatin remodelers. However, we did not observe corresponding upregulation in the expression of genes encoding the TFs belonging to these clusters (Supplementary Data 5, Supplementary Data 11), suggesting that a different mechanism might affect their activity.

We noticed that many motif clusters with increased accessibility in the neurons of high AI rats have decreased accessibility in oligodendrocytes (Fig. 5d-g). Prominent among these motif clusters are those containing FOX and RFX motifs (Fig. 5d-g).

Several motif clusters also have opposite effects between excitatory and inhibitory neurons. SOX motifs have decreased accessibility in high AI rats in excitatory neurons but increased accessibility in all other major cell types including inhibitory neurons (Fig. 5d). MEF2 and Fos (AP1) motifs all have increased accessibility in the excitatory neurons of high AI rats but decreased accessibility in inhibitory neurons (Fig. 5d). AP1 and MEF2 motifs are of particular interest because they are associated with addiction[93–96] and their expression changes in the brain following chronic exposure to cocaine and other drugs[97–101]. Consistent with these results, we observed that the expression of TFs of the AP1, including Fosl1, Fos, Jun, Junb, and Jund, was decreased in high versus low AI rats (Fig. S24), suggesting that differences in their expression level affect their transcriptional activity. While our analysis cannot pinpoint the precise TFs involved, it implicates many motif clusters that are associated with addiction-like behaviors across thousands of regulatory regions and in a cell type-specific manner.

Accessible chromatin regions harbor cell type-specific regulatory elements[102,103], and enrichment analyses that measure intersections between ATAC-seq peaks and GWAS signals can yield insight into the mechanisms by which genetic variants confer risk[104]. However, cell type-specific measurements of chromatin accessibility are difficult to obtain from human brain tissues. To assess whether our rat snATAC-seq data is meaningful for interpreting human addiction-related traits, we mapped the accessible chromatin peaks to the human reference genome and performed cell type-specific LD score regression[105]. We chose to use summary statistics from well-powered GWAS for alcohol and tobacco use[106,107] because there is significant genetic overlap among GWAS for all known substance use disorders[108] and because available GWAS for cocaine use disorder are much smaller and less powerful. We found significant enrichments (FDR<10%) of SNP heritability in every trait tested in almost every cell type (Fig. 5h), with the most significant enrichments in neurons, astrocytes, oligodendrocytes and OPCs. Overall, these results support the hypothesis that, despite the millions of years of evolution separating humans and rats, the regulatory architecture of HS rats is relevant for human addiction-related traits.

Discussion

To better understand the molecular basis of addiction and illuminate long-term changes in gene regulation and chromatin accessibility associated with chronic drug use, we have generated an atlas of single-cell gene expression and chromatin accessibility in the amygdala of rats that showed divergent cocaine addiction-like behaviors after a prolonged period of abstinence. Our dataset is the largest resource of cell types in the mammalian amygdala, with over 163,000 nuclei in our snRNA-seq dataset and 81,000 nuclei in our snATAC-seq dataset (Fig. 2a-b). The snATAC-seq dataset provides the first map of cell type-specific regulatory elements in the amygdala, which has allowed us to identify TF motifs that may drive addiction-related processes.

Previous single cell transcriptomic studies have focused on the effects of acute passive treatment with psychoactive drugs in rodents[37,38], which cannot fully capture the motivational processes underlying addiction. In contrast, our behavioral protocol involves extended access to cocaine IVSA and reflects several key aspects of cocaine addiction, including escalation of drug use, enhanced motivation for drug seeking and taking, and persistent drug use despite adverse consequences, which might reflect compulsive-like drug consumption[109]. In addition, using an outbred population of rats with divergent addiction-like traits allowed us to correlate molecular differences not only a high AI phenotype, which reflects vulnerability to severe addiction-like phenotypes, but also to a low AI phenotype, which reflects resiliency to developing behaviors that are hallmarks of addiction. Thus, our study is the first to examine long-term molecular changes in distinct brain cell populations following abstinence from chronic voluntary cocaine use in vulnerable and resilient rats.

One striking finding from our study is that there were thousands of significant cell type-specific differences in gene expression and chromatin accessibility between high and low AI rats, with strong biases in the direction of regulation of open chromatin regions in several major cell types (Fig. S16, S17, S21). Most of these differences were small, which suggests that cocaine addiction-related behaviors may result from the combined action of many small effects on gene expression and chromatin accessibility. Because the HS rats are genetically diverse, the molecular differences between high and low AI rats could arise from genetic differences or from the consumption of different quantities of cocaine. These results are consistent with a polygenic model wherein addiction-like behaviors would result from the collective action of a large number of genetic risk loci with small individual effects. This is a plausible explanation because of the high genetic diversity in the HS rats and because complex traits in humans are highly polygenic[105,110]. Further support for this hypothesis comes from the observation that the majority of DEGs have eQTLs identified in HS rat brains[70] (Fig. S17), including DEGs such as *Kcnq3, Fkbp5* and *Sgk1* (Fig. 3a-e).

Alternatively, the effects could be mediated by a relatively small number of TFs that affect many downstream genes and chromatin sites. Because some of the motifs with the strongest chromatin accessibility differences (Fig. 5e-h) are recognized by pioneer TFs (e.g. BHLH, Sox, Fox), it is tempting to speculate that widespread differences in accessibility are due to pioneer

TFs, which have an intrinsic ability to modify chromatin[111]. These explanations are not mutually exclusive and it is likely that some differences are caused by eQTLs while others are caused by differences in the activity of upstream regulators (which themselves may be affected by genetics or other factors).

In an effort to uncouple pre-existing genetically controlled gene expression differences from cocaine-induced neuroadaptations, we performed an analysis comparing our observed DEGs to differences in expression obtained from genotype-based prediction models. This allowed us to leverage the genotype data from our cohort of genetically diverse HS rats. We found significant correlations in observed versus predicted differential gene expression between high vs. low AI rats, suggesting that genetics does play a role in long-term transcriptional neuroadaptations that are observed following cocaine use. While the correlation metrics we obtained from our analysis are modest, this is expected due to three limitations of the predictive model. First, the models are trained on whole brain tissue and do not have the same cell type-specific resolution as our snRNA-seq data. Second, the size of the cohort on which the predictive models were trained was quite modest. Third, the models are only capable of capturing a small fraction of variation in expression and do not account for other influences on gene expression. Finally, it is likely that the DEGs we discovered are biased towards highly expressed genes, and eQTLs are less detectable in genes with very low expression. While these limitations make it difficult to quantify how much of the variance in expression is due to genetics, it establishes that at least some of the differences are due genetic variation (Fig. S18). To properly uncouple pre-existing genetically controlled gene expression differences from cocaine-induced neuroadaptations would require a larger datasets of genotyped rats. One way this could be accomplished is through the use of polygenic risk scores for addiction-related traits, which will become possible as more rat behavioral GWAS are completed[43,45–47,112].

Human and animal studies have provided genetic and behavioral evidence that alterations in GABAergic transmission are involved in addiction[2,113–117]. Consistent with prior findings showing that GABAergic transmission is enhanced following excessive cocaine use[118], our differential gene expression analysis showed enrichment of genes belonging to the GABAergic synapse pathway (Fig. 3f) and our electrophysiology results provided evidence for enhanced GABAergic transmission in the high AI rats (Fig. 4b). Moreover, we found that inhibition of GLO1, the enzyme responsible for MG metabolism, normalizes electrophysiological (Fig. 4c-f) and behavioral differences (Fig. 4h) associated with severe addiction-like behaviors. Specifically, while pBBG normalized the increased GABA transmission in electrophysiological recordings for both low and high AI rats (Fig. 4c), it had a normalizing effect on the drug-seeking behaviors in high AI rats but not low AI rats (Fig. 4h). This suggests that the inhibitory effects of pBBG on relapse-like behaviors depend on a given threshold of GABAergic transmission. These results corroborate previous findings that MG acts as an endogenous competitive agonist for $GABA_A$ receptors[113,119]. $GABA_A$ receptor agonists used in the context of cocaine-seeking behavior have shown contrasting results leading to both reduction or increase in cocaine-seeking behaviors[120–128]. Since MG is generated in proportion to glycolytic activity of nearly every cell and does not accumulate in synaptic vesicles, it diffuses and may activate $GABA_A$ receptors at synaptic and extra synaptic sites; thus, manipulating the endogenous levels of MG by GLO1 inhibition probes

a mechanism of $GABA_A$ receptor regulation that is fundamentally different from the canonical modulation of synaptic $GABA_A$ receptors. In our study, electrophysiological recordings suggest that there is an increase in GABAergic transmission without changes in postsynaptic currents in the CeA; thus, we speculate that MG-based pharmacological manipulations may alter presynaptic $GABA_A$ receptor function, reducing GABA release at inhibitory terminals and suppressing inhibitory connections within the CeA. Consistently, previous studies demonstrated that the activation of presynaptic $GABA_B$ receptors suppresses inhibitory connection within the CeA[84] and that negative regulation of GABAergic transmission can occur through a presynaptic mechanism[85]. An alternative scenario is that the magnitude of effects is not sufficient to cause detectable changes in amplitude. Overall, these results offer a promising pharmacological target for improving therapeutic approaches for cocaine addiction that was identified by our single cell analysis of the amygdala in high and low AI rats.

While the pharmacological inhibition experiments are not cell type-specific, the pathway enrichment analysis of the transcriptomic data suggest that GABAergic synapse-related genes may be specific to Cck+Vip+ and Nos1+ subtypes of inhibitory neurons. Previous studies manipulating GLO1 activity directly in the mouse amygdala by transgenic expression of *Glo1* or MG microinjection were sufficient to reduce anxiety-like behaviors[129]. Future experiments targeting specific subregions or cell types of the amygdala will be necessary to further characterize the effects of GLO1 inhibition on cocaine addiction-related phenotypes.

The results from the GLO1 inhibition experiments indicate a close connection between localized energy metabolism and neurotransmission[130]. Moreover, genes which are differentially regulated in high versus low AI rats are enriched in pathways related to energy metabolism, including glycolysis, pyruvate metabolism, and oxidative phosphorylation (Fig. 3f). Most notably, the expression levels of genes related to oxidative phosphorylation, which determines cellular ATP levels[131], are altered across most amygdalar cell types. Not only is ATP crucial for sustaining electrophysiological activity and cell signaling in the brain[132,133], but it is also required for ATP-dependent chromatin remodeling events initiated by pioneer TFs[134]. This could potentially explain why excitatory and inhibitory neurons show opposite directions of regulation in chromatin accessibility (Fig. S21) and in the enrichment of DEGs in the oxidative phosphorylation pathway (Fig. 3f). In combination, these observations suggest that an altered metabolic state within the amygdala impacts multiple cellular processes that are involved in vulnerability to and development of addiction. Future experiments that directly manipulate the expression of specific metabolic enzymes or pioneer TFs in a cell type-specific manner will be necessary to fully elucidate their role in addiction.

In conclusion, the cellular atlas created by this study is a valuable resource for understanding cell type-specific gene regulatory programs in the amygdala and their role in the development of cocaine addiction-related behaviors. Our results emphasize the contribution of cellular energetics and the $GABA_A$-mediated signaling to the enduring effects of cocaine use, which led us to perform experiments that manipulate $GABA_A$ transmission via the pharmacological inhibition of GLO1 and identify a novel potential target for treatment of cocaine addiction. We

anticipate that future studies will utilize our data to further investigate novel cell type-specific mechanisms involved in addiction.

Methods

Experimental

Animals

All protocols were reviewed and approved by the institutional Animal Care and Use Committee at the University of California San Diego. HS rats (Rat Genome Database NMcwiWFsm #13673907, sometimes referred to as N/NIH) which were created to encompass as much genetic diversity as possible at the NIH in the 1980's by outbreeding eight inbred rat strains (ACI/N, BN/SsN, BUF/N, F344/N, M520/N, MR/N, WKY/N and WN/N) were provided by Dr. Leah Solberg Woods (Wake Forest University School of Medicine). To minimize inbreeding and control genetic drift, the HS rat colony consists of 64 or more breeder pairs and is maintained using a randomized breeding strategy, with each breeder pair contributing one male and one female to subsequent generations. To keep track of the rats, their breeding, behavior, organs and genomic info, each rat received a chip with an RFID code. Rats were shipped at 3-4 weeks of age, kept in quarantine for 2 weeks and then housed two per cage on a 12 h/12 h reversed light/dark cycle in a temperature (20-22°C) and humidity (45-55%) controlled vivarium with ad libitum access to tap water and food pellets (PJ Noyes Company, Lancaster, NH, USA). We used 46 HS rats for the behavioral experiments presented in Fig. 1, of which 20 male rats (high and low AI) were used for the generation of snRNA-seq and snATAC-seq data, along with 11 naive male rats. Additionally, 26 of these 46 behaviorally phenotyped rats (13 female, 13 male) were used for the cue-induced reinstatement experiments. For snRNA-seq, we used 19 male rats (6 high AI, 6 low AI, 7 naive). For the snATAC-seq, we used 12 male rats (4 high AI, 4 low AI, 4 naive). In addition, we used a different cohort of 15 female and male rats (5 high AI, 5 low AI, 5 naive) for the electrophysiology experiments.

Drugs

Cocaine HCl (National Institute on Drug Abuse, Bethesda, MD, USA) was dissolved in 0.9% saline (Hospira, Lake Forest, IL, USA) and administered intravenously at a dose of 0.5 mg/kg/infusion as described below. pBBG was synthesized in the laboratory of Prof. Dionicio Siegel (University of California San Diego, Skaggs School of Pharmacy and Pharmaceutical Sciences). pBBG was dissolved in a vehicle of 8% dimethylsulfoxide, 18% Tween-80, and 74% distilled water and administered intraperitoneally 30 minutes before the test session.

Brain Samples

Brain tissues were obtained from the cocaine brain bank at UCSD[39], which collects tissues from HS rats that are part of an ongoing study of addiction-like behavior[43]. We used 31 HS rats for

generating the single-nucleus sequencing data reported in this study, which included 20 rats that had low or high AI for cocaine addiction-related behaviors, using behavioral methods previously described[48] were kept in their home cages and never subjected to the catheter implantation or the behavioral protocol for cocaine IVSA. Brain tissues were collected after four weeks of abstinence from cocaine self-administration, which has been used in prior studies to examine long-lasting effects of self-administration[47,135–140]. Brain tissues were extracted and snap-frozen (at −30°C). Cryosections of approximately 500 microns (Bregma -1.80 - 3.30mm) were used to dissect the amygdala on a −20°C frozen stage, including the CeA, BLA, and medial amygdala from both hemispheres. Punches from three sections were combined for each rat. In addition, 6 ACI/EurMcw rats were used for the dissection of the CeA and BLA.

Single-cell library preparation, sequencing, and alignment

snRNA-seq libraries from the whole amygdala tissues were performed by the Center for Epigenomics, UC San Diego using the Droplet-based Chromium Single-Cell 3' solution (10x Genomics, v3 chemistry). Briefly, frozen tissue was homogenized via glass dounce. Nuclei were then resuspended in 500 µL of nuclei permeabilization buffer (0.1% Triton-X-100 (Sigma-Aldrich, T8787), 1X protease inhibitor, 1 mM DTT, and 1U/µL RNase inhibitor (Promega, N211B), 2% BSA (Sigma-Aldrich, SRE0036) in PBS). Sample was incubated on a rotator for 5 min at 4°C and then centrifuged at 500 rcf for 5 min (4°C, run speed 3/3). Supernatant was removed and pellet was resuspended in 400 µL of sort buffer (1 mM EDTA 0.2 U/µL RNase inhibitor (Promega, N211B), 2% BSA (Sigma-Aldrich, SRE0036) in PBS) and stained with DRAQ7 (1:100; Cell Signaling, 7406). Up to 75,000 nuclei were sorted using a SH800 sorter (Sony) into 50 µL of collection buffer consisting of 1 U/µL RNase inhibitor in 5% BSA; the FACS gating strategy sorted based on particle size and DRAQ7 fluorescence. Sorted nuclei were then centrifuged at 1000 rcf for 15 min (4°C, run speed 3/3) and supernatant was removed. Nuclei were resuspended in 35 µL of reaction buffer (0.2 U/µL RNase inhibitor (Promega, N211B), 2% BSA (Sigma-Aldrich, SRE0036) in PBS) and counted on a hemocytometer. 12,000 nuclei were loaded onto a Chromium Controller (10x Genomics). Libraries were generated using the Chromium Single-Cell 3′ Library Construction Kit v3 (10x Genomics, 1000075) with the Chromium Single-Cell B Chip Kit (10x Genomics, 1000153) and the Chromium i7 Multiplex Kit for sample indexing (10x Genomics, 120262) according to manufacturer specifications. cDNA was amplified for 12 PCR cycles.

For snATAC-seq libraries from the whole amygdala tissues, nuclei were purified from frozen tissues using an established method[141]. Briefly, frozen amygdala tissue was homogenized using a 2 ml glass dounce with 1 ml cold 1x Homogenization Buffer (HB). The cell suspension was filtered using a 70 µm Flowmi strainer (BAH136800070, Millipore Sigma) and centrifuged at 350g for 5 min at 4°C. Nuclei were isolated by iodixanol (D1556, Millipore Sigma) density gradient. The nuclei iodixanol solution (25%) was layered on top of 40% and 30% iodixanol solutions. Samples were centrifuged in a swinging bucket centrifuge at 3,000g for 20 min at 4°C. Nuclei were isolated from the 30-40% interface. Libraries were generated using the Chromium

Next GEM Single Cell ATAC v1.1 (10x Genomics, PN-1000175) with the Chromium Next GEM Chip H Single Cell Kit (10x Genomics, 1000162) and the Chromium i7 Multiplex Kit for sample indexing (10x Genomics, 1000212) according to manufacturer specifications. DNA was amplified for 8 cycles.

For snRNA libraries from BLA and CeA, frozen brain tissues were obtained from the ACI/EurMcw rat strain, one of the HS rat founder strains. For nuclei isolation, brain punches from 3 rats for each region were pooled and homogenized in homogenization buffer (0.26 M sucrose, 0.03 M KCl, 0.01 M MgCl2, 0.02 M Tricine-KOH pH 7.8, 0.001 M DTT, 0.5 mM spermidine, 0.15 mM Spermine, 0.3% NP40) using with 1ml glass Dounce homogenizers. The homogenate was filtered with a 70-um strainer filter (SP Bel-Art, cat no 136800070) and centrifuged for 5 minutes at 350 RCF. The nuclei were purified with an iodixanol gradient (Sigma-Aldrich # 92339-11-2) by layering a 25% Iodixanol-nuclei mixture on top of 30% and 40% Iodixanol solutions. After centrifugation at 4°C 3,000 RCF for 20 minutes, nuclei were collected from the 30-40% interface. Nuclei were washed in ATAC-RSB-Tween buffer (0.01 M Tris-HCl pH 7.5, 0.01 M NaCl, 0.003 M MgCl2, 0.1% Tween-20) and then resuspended in 1X nuclei buffer (10X genomics, PN 2000207). 12,000 nuclei were loaded on the 10X Genomics Chromium Controller for GEM generation. RNAse inhibitors (Roche Diagnostics, # 03335402001) were added to all buffers (1U/ul). snRNA-seq library was performed using the Chromium Next GEM Single Cell Multiome Reagent Kit A (# 1000282) following Chromium Next GEM Single Cell Multiome ATAC + Gene Expression Reagent Kits User Guide (10X Genomics). After the transposition reaction, nuclei were encapsulated and barcoded. Next-generation sequencing libraries were constructed following the User Guide.

For each library type, SPRISelect reagent (Beckman Coulter, B23319) was used for size selection and clean-up steps. Final library concentration was assessed by Qubit dsDNA HS Assay Kit (Thermo-Fisher Scientific) and post library QC was performed using Tapestation High Sensitivity D1000 (Agilent) to ensure that fragment sizes were distributed as expected. Final libraries were sequenced using the NovaSeq6000 (Illumina).

Behavioral experiments

Intravenous catheterization and behavioral testing of rats used for the generation of snRNA-seq and snATAC-seq were carried out using an established protocol of extended access to cocaine IVSA, progressive ratio (PR) testing, and foot shock, as reported previously[39,48,49]. Briefly, after surgical implantation of intravenous catheters and a week of recovery, HS rats were trained to self-administer cocaine (0.5 mg/kg/infusion) in 10 short access (ShA) sessions (2h/day, 5 days per week). Next, the animals were allowed to self-administer cocaine in 14 long access (LgA) sessions (6h/day, 5 days/week) to measure the escalation of drug intake (Fig. 1e). Following the escalation phase, rats were screened for motivation using the PR test and for persistent drug-seeking despite adverse consequences using contingent foot-shock. The breakpoint (Fig. 1f) was defined as the maximal number of presses completed before a 60-minute period during which a rat does not complete the next schedule. Rats were classified as vulnerable (high AI), defined by having high addiction-like behavior, versus resilient (low AI), defined as having low

addiction-like behavior, via a median split[51,52]. AI was computed by averaging normalized measurements (z-scores) for the three behavioral tests: escalation of drug intake, motivation, and compulsive-like behavior, or drug taking despite adverse consequences[142] (Fig. 1c-d). The z-scores were calculated as $Z = (x-\mu)/\sigma$, where x is the raw value, μ is the mean of the cohort, and σ is the standard deviation of the cohort. Brain tissues were collected after four weeks of abstinence. For the pBBG studies, we used rats with low and high AI distinct from those used for the snRNA-seq and snATAC-seq experiments. Four weeks after the last drug self-administration session, the rats were placed back in the self-administration chambers without the availability of cocaine. The number of responses to the previous drug-paired lever (cocaine seeking behavior) was measured 30 minutes after intraperitoneal injection of pBBG (15 mg/kg/ml) or its vehicle, in a Latin square design. The 30 minutes time point was selected based on a previous study[86]. Data were analyzed using Prism 9.0 software (GraphPad, San Diego, CA, USA). Self-administration data were analyzed using repeated-measures analysis of variance (ANOVA) or mixed effect model followed by Bonferroni post-hoc tests when appropriate. For pairwise comparisons, data were analyzed using the unpaired *t*-test. The data are expressed as mean ± SEM unless otherwise specified. Values of $p < 0.05$ were considered statistically significant.

Electrophysiology

Slices of the CeA were prepared from rats after 4 weeks of protracted abstinence from cocaine IVSA following the same behavioral protocol described above or age-matched naive rats. High AI (n=5), low AI (n=5) and naive (n=5) rats were used for patch clamp baseline recordings. These rats were distinct from those used for snRNA-seq and snATAC-seq. Slices from each group were also used to record iPSCs after pBBG treatment. The naive rats received sham IV surgery. The rats were deeply anesthetized with isoflurane and brains were rapidly removed and placed in oxygenated (95% O_2, 5% CO_2) ice-cold cutting solution that contained 206 mM sucrose, 2.5 mM KCl, 1.2 mM NaH_2PO_4, 7 mM $MgCl_2$, 0.5 mM $CaCl_2$, 26 mM $NaHCO_3$, 5 mM glucose, and 5 mM Hepes. Transverse slices (300 μm thick) were cut on a Vibratome (Leica VT1200S; Leica Microsystems) and transferred to oxygenated artificial cerebrospinal fluid (aCSF) that contained 130 mM NaCl, 2.5 mM KCl, 1.2 mM NaH_2PO_4, 2.0 mM $MgSO_4 \cdot 7H_2O$, 2.0 mM $CaCl_2$, 26 mM $NaHCO_3$, and 10 mM glucose. The slices were first incubated for 30 min at 35°C and then kept at room temperature for the remainder of the experiment. Individual slices containing CeA were transferred to a recording chamber that was mounted on the stage of an upright microscope (Olympus BX50WI). The slices were continuously perfused with oxygenated aCSF at a rate of 3 mL/min. Neurons were visualized with a 60X water-immersion objective (Olympus), infrared differential interference contrast optics, and a charge coupled device camera (EXi Blue; QImaging). Whole-cell recordings were performed using a Multiclamp 700B amplifier (10 kHz sampling rate, 10 kHz low-pass filter) and Digidata 1440A and pClamp 10 software (Molecular Devices). Patch pipettes (4–6 MΩ) were pulled from borosilicate glass (Warner Instruments) and filled with 70 mM $KMeSO_4$, 55 mM KCl, 10 mM NaCl, 2 mM $MgCl_2$, 10 mM Hepes, 2 mM Na-ATP, and 0.2 mM Na-GTP. Pharmacologically isolated sIPSCs were recorded in the presence of the glutamate receptor blockers, CNQX (Tocris #0190) and APV (Tocris #189), and the GABA-B receptor antagonist CGP55845 (Tocris #1246). Experiments

with a series resistance of >15 MΩ or >20% change in series resistance were excluded from the final dataset. pBBG (2.5uM) was acutely applied in the bath. The frequency, amplitude, and kinetics of sIPSCs were analyzed using semi automated threshold-based mini detection software (Easy Electrophysiology) and visually confirmed. Data were analyzed using Prism 9.0 software (GraphPad, San Diego, CA, USA) with one-way ANOVA followed by post hoc Tukey HSD test or with paired t-tests. The data are expressed as mean ± SEM unless otherwise specified. Values of $p < 0.05$ were considered statistically significant.

Computational

Alignment of snRNA-seq and snATAC-seq reads

Raw base call (BCL) files were used to generate FASTQ files using Cell Ranger 3.1.0 for snRNA-seq data, Cellranger ATAC v.2.0.0 for snATAC-seq data, and Cell Ranger ARC v.2.0.0 for processing Chromium Single Cell Multiome ATAC + Gene Expression sequencing data. For demultiplexing raw base call (BCL) files generated by the sequencers into FASTQ files, we used the `cellranger mkfastq` command for RNA-seq reads, `cellranger-atac mkfastq` for ATAC-seq reads, and `cellranger-arc mkfastq` for the CeA and BLA samples which were generated using the multiome kit[143,144]. Next, we used `cellranger count` and `cellranger-atac count` to align the snRNA-seq and snATAC-seq reads, respectively, to a custom rat reference genome based on the rn6 reference genome downloaded from the UCSC genome browser[145–147]. The reference genome files for cell ranger were created from FASTA and genome annotation files for Rattus norvegicus Rnor_6.0 (Ensembl release 98)[148] and JASPAR2022 motifs[149]. BLA and CeA samples were aligned to the same reference genome using `cellranger-arc count`. We then filtered cells based on quality control metrics and performed barcode and UMI counting for the RNA-seq and ATAC-seq reads.

Quality control and preprocessing of snRNA-seq data

All snRNA-seq preprocessing was performed with Seurat v3.2.3[56]. For each sample, we loaded the filtered feature barcode matrices containing only detected cellular barcodes returned by `cellranger count` into Seurat. We computed the number of unique genes detected in each cell (nFeature_RNA); the total number of molecules detected within a cell (nCount_RNA); and the percentage of reads mapping to the mitochondrial genome (percent.mt) (Fig. S1-3, Supplementary Data 1, Supplementary Data 3). nFeature_RNA is informative because low-quality cells or empty droplets will typically have very low numbers of detected genes while doublets or multiplets will exhibit very high gene counts. nCount_RNA is a metric that correlates with nFeature_RNA. We examined percent.mt because low-quality or dying cells typically exhibit a high degree of mitochondrial contamination. We removed all cells for which the value of any of these metrics was more than three standard deviations from the mean within the sample ($x > \mu \pm 3\sigma$). Next, we normalized the count data for each sample using sctransform[150] with percent.mt as a covariate.

Integrating snRNA-seq data across samples and clustering

To integrate snRNA-seq data across all of our samples, we used reciprocal principal component analysis (RPCA), as implemented in Seurat[56,151]. First, we identified 2000 highly variable features (genes) across all of the samples to use as integration features using the `SelectIntegrationFeatures()` function, which we passed as anchor features (`anchor.features`) to the `PrepSCTIntegration()` function. Next, we performed dimensionality reduction with PCA on each sample using `RunPCA()`. After this, we ran the `FindIntegrationAnchors()` function to find a set of anchors between the list of Seurat objects from all of our samples using the same anchor features passed to `PrepSCTIntegration()`, specifying RPCA as the dimensional reduction method to be performed for finding anchors (`reduction = rpca`) and the first 30 RPCA dimensions to be used for specifying the k-nearest neighbor search space. Two rats (1 high AI, 1 low AI) were used as reference samples for the integration. We used the resulting anchor set to perform dataset integration across all of our samples using `IntegrateData()`. We clustered the integrated dataset by constructing a K-nearest neighbor (KNN) graph using the first 30 PCs followed by the Louvain algorithm, implemented in Seurat using the `FindNeighbors()` function followed by `FindClusters()`. Finally, we ran PCA once again on the integrated dataset and visualized the data using uniform manifold approximation and projection (UMAP). Visualization of the integrated data in two-dimensional space indicated that batch correction was successful (Fig. S9a-c). To compare CeA and BLA subregion samples with the whole amygdala, we subsampled whole amygdala samples from the naïve rats in our study and performed the same integration technique. The integrated subregion data was visualized using UMAP.

Cell type assignment for snRNA-seq data

We identified marker genes of each cluster in our integrated snRNA-seq dataset using MAST[152], implemented with the `FindMarkers()` function in Seurat. Cell type identities were assigned based on expression of known marker genes of cell types known to be found in the amygdala.

Cell type-specific gene expression analysis for snRNA-seq data

Within each cell type, we tested for DEGs between the high AI rats and the low AI rats. We used the negative binomial test[88,89] implemented with the `FindMarkers()` function in Seurat to identify differential expression between groups, using percent.mt and the library prep date as covariates. We used the avg_log2FC value returned by the `FindMarkers()` function as an estimate of effect size. We did not pre-filter genes for testing based on log-fold change or minimum fraction of cells in which a gene was detected. This approach allowed us to detect weaker signals because we tested all observed genes in the dataset. Multiple testing correction was performed using the Benjamini-Hochberg method and we used a false discovery rate of 10% as a significance threshold (FDR<10%). Permutation tests were performed using the same methods, covariates, and filtering options but with shuffled addiction index labels. Results from permuted and unpermuted data were compared by visualizing the distributions of uncorrected p-values with QQ-plots (Fig. S15, Supplementary Data 6).

We used ClusterProfiler[153] to perform gene set enrichment analysis (GSEA) of KEGG pathways for DEGs from each cell type. A ranked list of the avg_logFC values for all genes evaluated with our negative binomial test was given as input to GSEA. Multiple testing correction for GSEA results was performed using Benjamini-Hochberg adjustment, with statistical significance assessed at a FDR<10%.

All rat eQTLs described in the paper come from the RatGTEx portal (https://ratgtex.org/download/). Specifically, we downloaded their table of conditionally independent cis-eQTLs, which only includes eQTLs passing a significance threshold of FDR<0.05. We examined cis-eQTLs in the following brain tissues: BLA, Brain, IL, LHb, NAcc, NAcc2, OFC, PL, PL2. For each cis-eQTL in the database, only the top associated SNP is given, but some genes have more than one cis-eQTL in a tissue, meaning there are multiple loci with statistically independent associations with the gene's expression. We measured enrichment of significant DEGs (FDR<10%) that also had eQTLS in the rat brain using the Chi-squared test, implemented using the `chisq.test()` function in R.

To obtain bootstrap distributions of DEG effect sizes, we resampled nuclei with replacement 1000 times. Resampling was performed separately for nuclei from high and low AI rats so that the sample size of each set remained consistent. For each bootstrap iteration we recorded the p-value and the coefficients for the hi/low AI condition from the negative binomial regression performed by Seurat's `FindMarkers()' function. We then rescaled the coefficient to be in units of log2 fold change. We note that the log2FC estimates obtained by this method correspond to the p-values, but differ slightly from Seurat's avg_log2FC estimates because Seurat's avg_log2FC calculations introduce a pseudocount and do not consider the effects of covariates. The distribution of resulting bootstrap fold-change estimates and q-values were visualized as violin plots using Plotly in Python (Fig. 3c-e).

Comparing observed gene expression differences to predicted gene expression differences based on cis-genetic variation

To estimate the genetic component of gene expression variation in the brain, conditionally independent cis-eQTLs and their allelic fold change (aFC) estimates for whole brain hemisphere tissue were downloaded from the RatGTEx Portal (https://ratgtex.org/download/). Using aFC as effect size, gene expression was predicted from genotypes using eQTL linear models[77] (https://github.com/PejLab/gene_expr_pred). Predicted relative expression was thus obtained for 26 rats whose genotypes were available, and only for genes with at least one significant cis-eQTL. Genes with zero-variance predictions were removed, resulting in predictions for 8,997 genes. To further prioritize genes by estimated prediction accuracy, gene expression was predicted for the same 339 rats that were used to map the whole brain hemisphere eQTLs. Pearson correlation r^2 was calculated between those predictions and observed log-TPM expression from the same rats. We then measured the difference between mean predicted expression in high vs low AI rats and compared it against the avg_logFC estimates obtained by Seurat's FindMarkers() function. Spearman's correlation coefficient (ρ) was calculated between the difference in mean predicted expression and the observed avg_logFC. We performed these

tests multiple times using different r^2 cutoffs for the gene expression prediction models to filter genes (Table. S3). Spearman's correlation coefficients (ρ) and the associated p-values were calculated using `scipy.stats.spearmanr()`. Confidence intervals were calculated using the formula $tanh(tanh^{-1}(\rho) \pm \frac{1.96}{\sqrt{N-3}})$. Spearman ρ confidence intervals were visualized using Plotly in Python.

Quality control and preprocessing of snATAC-seq data

All snATAC-seq data preprocessing was performed with MACS2[87] (for peak calling) and Signac[57]. Although peak calling is performed during alignment by `cellranger-atac count`, we chose to call peaks separately using MACS2 because Cell Ranger's peak calling function has been observed to merge multiple distinct peaks into a single region[154]. To minimize loss of informative features for clustering and downstream analysis, we first called peaks on the snATAC-seq BAM files for each rat with MACS2 (`macs2 callpeak -t {input} -f BAM -n {sample} --outdir {output} {params} --nomodel --shift -100 --ext 200 --qval 5e-2 -B --SPMR`). We confirmed that MACS2 calls more peaks and peaks with smaller widths compared to Cell Ranger (Fig. S25). Next, we merged overlapping peaks across all of our samples to generate a combined peak set using BEDtools[155] (`bedtools merge`). We generated a new peak by barcode matrix for each sample using this combined peak set and all detected cellular barcodes using the `FeatureMatrix()` function in Signac. We used these new matrices to create ChromatinAssay objects in Signac with the BSgenome.Rnorvegicus.UCSC.rn6[146] reference genome using the `CreateChromatinAssay()` function. From these ChromatinAssay objects we created Seurat objects with `CreateSeuratObject()`, which are compatible with functions from the Seurat package. We computed several quality control metrics for each sample: nucleosome banding pattern (nucleosome_signal); transcriptional start site (TSS) enrichment score (TSS.enrichment); total number of fragments in peaks (peak_region_fragments); and fraction of fragments in peaks (pct_reads_in_peaks) (Fig. S4-6, Supplementary Data 2, Supplementary Data 4). We removed all cells for which the value of any of these metrics was more than two standard deviations from the mean within the sample ($x > \mu \pm 2\sigma$). We removed one rat (FTL_463_M757_933000320046135) from our dataset, due to the very low number of detected fragments per cell in this sample (Fig. S26).

Integrating snATAC-seq data across samples and clustering

Each sample was normalized using term frequency-inverse document frequency (TF-IDF) followed by singular value decomposition (SVD) on the TF-IDF matrix using all features (peaks)[57,154]. The combined steps of TF-IDF followed by SVD are known as latent semantic indexing (LSI)[156,157]. Non-linear dimensionality reduction and clustering were performed using UMAP and KNN following the same procedure used, respectively, just as we did for the snRNA-seq data. We merged the data across all samples within Signac and repeated the process of LSI in the same manner as it was applied to individual samples. We then integrated the merged dataset using Harmony[158] implemented by Signac, integrating over the sample library variable to account for the effects of different sequencing libraries used for different samples. We observed successful reduction of batch effects following integration Fig. S9d-f. We once again performed

non-linear dimensionality reduction and clustering with UMAP and KNN, respectively. Notably, LSI, UMAP and KNN are used for visualization purposes; raw counts were used for downstream differential accessibility analyses.

Label transfer and cell type assignment for snATAC-seq data

We created a gene activity matrix for the integrated snATAC-seq data using the `GeneActivity()` function in Signac. This counts the number of fragments per cell overlapping the promoter region of a given gene and uses that value as a gene activity score. Gene activity serves as a proxy for gene expression as gene expression is often correlated with promoter accessibility. The gene activity scores were log normalized using the `NormalizeData()` function in Seurat with the normalization method set to `LogNormalize` and the scaling factor set to the median value of nCount_RNA across all cells, based on the gene activity scores. Cell type identities were assigned by integrating the snATAC-seq data with the integrated snRNA-seq data and performing label transfer[56] as described in Signac. Briefly, this approach identifies shared correlation patterns in the gene activity matrix and the scRNA-seq dataset to identify matched biological states across the two modalities. The process returns a classification score for each cell for each cell type defined in the scRNA-seq data. Each cell was assigned the cell type identity with the highest prediction score. Additionally, by identifying matched cells in the snRNA-seq dataset, we were able to impute RNA expression values for each of the cells in our snATAC-seq dataset. This enabled us to perform correlative analyses of chromatin accessibility and gene expression in later downstream analyses, as it produced a pseudo-multimodal dataset.

Differential chromatin accessibility analysis of snATAC-seq data

Similar to our differential analyses of the snRNA-seq data, we tested for differentially accessible genomic regions between nuclei from the high versus low AI rats within each cell type. We used the negative binomial test[150,159] implemented with the `FindMarkers()` function from Seurat to model the raw snATAC-seq count data using peak_region_fragments, library batch date, and rat sample ID as covariates. Multiple testing correction was performed using Benjamini-Hochberg adjustment and a false discovery rate below 10% (FDR<10%) was used to determine statistical significance. Permutation tests were performed in the same manner as for the differential gene expression analyses (using the same statistical test and covariates with shuffled addiction index labels).

Partitioned heritability analysis

We downloaded summary statistics for the Liu et al. 2019 GWAS of tobacco and alcohol use[106] and used the munge_sumstats.py script from LD Score (LDSC)[105] to parse the summary statistics file into the proper format for downstream analyses. We used the sets of significant differential peaks (FDR<10%) for each cell type as foreground peaks and DNaseI hypersensitivity profiles for 53 epigenomes from ENCODE Honeybadger2. We used the UCSC liftOver tool to convert the foreground peaks from rn6 to hg19. There was no need to lift over the background peaks as Honeybadger2 is already in hg19. Next, we generated partitioned LD

scores for the background and foreground regions. We used the make_annot.py script to make annotation files and the ldsc.py script to compute annotation-specific LD scores. We used the European 1000 Genomes Phase 3 PLINK[160] files to compute the LD scores. Finally, using the baseline model and standard regression weights from the LDSC Partitioning Heritability tutorial, we ran a cell type-specific partitioned heritability analysis with the LD scores we computed.

Annotation of accessible chromatin regions

Before performing any differential analyses, we first used the annotatePeaks.pl script from the HOMER suite to annotate accessible chromatin regions and significant differential peaks (FDR<10%) for each cell type in our integrated dataset[161]. For each cell type, we performed a Fisher's Exact Test to measure the enrichment of genomic regions annotated as a promoter region within the differential peaks compared to the set of all peaks in the dataset and observed significant results for all cell types tested. Specifically, we compared the ratio of peaks annotated as promoter regions to non-promoter regions in the significant differential peaks (FDR<10%) versus all other peaks.

Fisher's Exact Tests

We first performed a Fisher's Exact Test to measure enrichment of DEGs (FDR<10%) with differentially accessible promoters. We defined the latter as the case where the promoter region of a gene overlaps a significant differentially accessible peak (FDR<10%). We obtained gene coordinates from the TxDb.Rnorvegicus.UCSC.rn6.refGene annotation package and defined promoter regions as being 1500 bases upstream and 500 bases downstream of the TSS (`promoters(genes(TxDb.Rnorvegicus.UCSC.rn6.refGene), upstream = 1500, downstream = 500)`). We then generated a confusion matrix from the following four values: the number of DEGs with differentially accessible promoters; the number of DEGs with non-differentially accessible promoters; the number of non-DEGs with differentially accessible promoters; and the number of non-DEGs with non-differentially accessible promoters. We then performed a Fisher's Exact Test to measure enrichment of differentially accessible peaks (FDR<10%) which were annotated as TSS/promoter regions by HOMER (annotatePeaks.pl). We generated a confusion matrix from the following four values: the number of differential peaks with a TSS/promoter annotation; the number of differential peaks without a TSS/promoter annotation; the number of non-differential peaks (FDR>10%) with a TSS/promoter annotation; and the number of non-differential peaks (FDR>10%) without a TSS/promoter annotation.

Measuring differential activity of transcription factors with chromVAR

We measured cell type specific motif activities using chromVAR to test for per motif deviations in accessibility between nuclei from high versus low AI rats. Motif data was pulled from the JASPAR2020 database, and integrated with snATAC-seq data using the `AddMotifs()` function in Signac. After adding motifs to our snATAC-seq dataset, we ran chromVAR with the `RunChromVAR()` wrapper in Signac. Differential analysis of chromVAR deviation scores was performed using the Wilcoxon rank-sum test between high AI rats versus lowly addicted rats within each cell type. Differential testing was performed using Seurat's `FindMarkers()` function

with the mean function set as `rowMeans()` to calculate average difference in deviation scores between groups. Multiple testing correction was performed using Benjamini-Hochberg adjustment and a false discovery rate below 10% (FDR<10%) was used to determine statistical significance. Motif clusters were defined using the provided cluster numbers from JASPAR's matrix clustering-results and the names of the clusters were annotated by hand based on which TFs were present in each cluster. When selecting clusters to visualize, we retrieved the top 50 motifs (FDR<10%) per cell-type and highlighted their respective clusters. Volcano plots and heatmap data were generated using Plotly in Python. Hierarchical ordering of heatmap clusters was generated with Plotly's `figure_factory.create_dendrogram()` function, which wraps the `cluster.hierarchy.dendrogram()` function in SciPy.

Data availability

The datasets generated in the current study are available through the Gene Expression Omnibus (GSE212417, token gpczagqerncrfmz).

The following publicly available datasets were used: Rattus norvegicus Ensembl v98 reference genome and genome assembly (Rnor_6.0); JASPAR2022 transcription factor binding profiles for vertebrates; ENCODE Honeybadger 2 ChIP-seq; 1000 Genomes European reference panel; Liu et al. 2019[106] GWAS for tobacco and nicotine addiction; RatGTEx Portal tissue-specific cis-eQTLs.

The behavioral data of HS rats are available at https://cgord.org/

Code availability

All code used to perform analyses in this paper can be found at https://github.com/mcvickerlab/sn_cocaine_rats.

Acknowledgements

We thank S. Preissl from the UC San Diego School of Medicine Center for Epigenomics for technical assistance with the snRNA-seq library preparation. We thank J. Hightower for assistance with figures preparation. We thank P. Montilla-Perez, L. Maturin and P. Schweitzer for technical assistance with sample collection and equipment maintenance. We thank Leah C. Solberg Woods for HS rats breeding colony management. This work was supported by the National Institutes of Health (NIH) (U01DA050239 to F.T.; F31DA056226 to J.L.Z.; U01DA043799 to O.G., P50DA037844 to A.A.P., R01GM140287 to P.M.). G.d.G. was supported by the Brain and Behavior Research Foundation 2020 Young Investigator Award and M.K. by the TDRP (T31KT1859 UC) grant. This publication includes data generated at the UC San Diego IGM Genomics Center utilizing an Illumina NovaSeq 6000 that was purchased with funding from the NIH (S10OD026929).

Author information

Authors and Affiliations

Bioinformatics and Systems Biology Program, University of California San Diego, La Jolla, CA, 92093, USA

Jessica L. Zhou, Graham McVicker

Integrative Biology Laboratory, Salk Institute for Biological Studies, La Jolla, CA, 92037, USA

Jessica L. Zhou, Aaron J. Ho, & Graham McVicker

Department of Psychiatry, University of California, San Diego, La Jolla, CA, 92092, USA

Giordano de Guglielmo, Marsida Kallupi, Apurva S. Chitre, Daniel Munro, Lieselot LG Carrete, Olivier George, & Abraham A. Palmer

Department of Medicine, University of California San Diego, La Jolla, CA 92093, USA

Hai-Ri Li & Francesca Telese

Department of Integrative Structural and Computational Biology, The Scripps Research Institute, La Jolla, CA, 92037, USA

Daniel Munro, Pejman Mohammadi

Center for Immunity and Immunotherapies, Seattle Children's Research Institute, Seattle, WA, 98145, USA

Pejman Mohammadi

Department of Pediatrics, University of Washington School of Medicine, Seattle, WA, 98195, USA

Pejman Mohammadi

Department of Genome Sciences, University of Washington, Seattle, WA, 98195, USA

Pejman Mohammadi

Institute for Genomic Medicine, University of California San Diego, La Jolla, CA 92093, USA

Abraham A. Palmer

Contributions

F.T. designed and coordinated the study. G.M. designed the overall bioinformatics analysis flow. J.L.Z. conducted bioinformatic analysis and data interpretation with inputs from F.T., G.M., and A.A.P.. A.J.H. conducted ChromVar analysis. O.G. and G.d.G. designed the behavioral protocol for cocaine IVSA. G.d.G. performed the behavioral experiments. M.K. performed the electrophysiological experiments. L.L.C. dissected the brain samples. H.L. performed snATAC-seq experiments. N.P. performed the snRNAseq experiments for the CeA and BLA. A.A.P., D.M. and P.M. coordinated and executed the gene expression predictions for naive HS rats using eQTL data. A.S.C. provided genotype data for exploratory analysis. J.L.Z., A.P., G.M. and F.T. wrote the manuscript with contributions from all authors.

Corresponding authors

Correspondence to Graham McVicker or Francesca Telese.

Ethics declarations

Competing interests

A.A.P. holds a patent related to the use of GLO1 inhibitors (US20160038559, active). The inventors of this patent are Dr. Abraham Palmer and Dr. Margaret Distler.

References

1. Janak PH, Tye KM. From circuits to behaviour in the amygdala. Nature. 2015 Jan 15;517(7534):284–292. PMCID: PMC4565157
2. Roberto M, Gilpin NW, Siggins GR. The Central Amygdala and Alcohol: Role of γ-Aminobutyric Acid, Glutamate, and Neuropeptides. Cold Spring Harb Perspect Med. 2012 Dec;2(12):a012195. PMCID: PMC3543070
3. Buffalari DM, See RE. Amygdala Mechanisms of Pavlovian Psychostimulant Conditioning and Relapse. In: Self DW, Staley Gottschalk JK, editors. Behavioral Neuroscience of Drug Addiction [Internet]. Berlin, Heidelberg: Springer; 2010 [cited 2022 Aug 4]. p. 73–99. Available from: https://doi.org/10.1007/7854_2009_18
4. Schumann CM, Bauman MD, Amaral DG. Abnormal structure or function of the amygdala is a common component of neurodevelopmental disorders. Neuropsychologia. 2011 Mar;49(4):745–759. PMCID: PMC3060967
5. Koob GF. Anhedonia, Hyperkatifeia, and Negative Reinforcement in Substance Use Disorders. In: Pizzagalli DA, editor. Anhedonia: Preclinical, Translational, and Clinical Integration [Internet]. Cham: Springer International Publishing; 2022 [cited 2023 Apr 21]. p. 147–165. Available from: https://doi.org/10.1007/7854_2021_288
6. Pickens CL, Airavaara M, Theberge F, Fanous S, Hope BT, Shaham Y. Neurobiology of the incubation of drug craving. Trends Neurosci. 2011 Aug;34(8):411–420. PMCID: PMC3152666
7. Kalivas PW, Volkow ND. The Neural Basis of Addiction: A Pathology of Motivation and Choice. AJP. American Psychiatric Publishing; 2005 Aug;162(8):1403–1413.
8. Kilts CD, Schweitzer JB, Quinn CK, Gross RE, Faber TL, Muhammad F, Ely TD, Hoffman JM, Drexler KPG. Neural Activity Related to Drug Craving in Cocaine Addiction. Archives of General Psychiatry. 2001 Apr 1;58(4):334–341.
9. Aerts T, Seuntjens E. Novel Perspectives on the Development of the Amygdala in Rodents. Front Neuroanat. 2021 Dec 9;15:786679. PMCID: PMC8696165
10. Arrigucci R, Bushkin Y, Radford F, Lakehal K, Vir P, Pine R, Martin D, Sugarman J, Zhao Y, Yap GS, Lardizabal AA, Tyagi S, Gennaro ML. FISH-Flow, a protocol for the concurrent detection of mRNA and protein in single cells using fluorescence in situ hybridization and flow cytometry. Nat Protoc. 2017 Jun;12(6):1245–1260. PMCID: PMC5548662
11. Ehrlich I, Humeau Y, Grenier F, Ciocchi S, Herry C, Lüthi A. Amygdala Inhibitory Circuits and the Control of Fear Memory. Neuron. Elsevier; 2009 Jun 25;62(6):757–771. PMID: 19555645
12. Ciocchi S, Herry C, Grenier F, Wolff SBE, Letzkus JJ, Vlachos I, Ehrlich I, Sprengel R, Deisseroth K, Stadler MB, Müller C, Lüthi A. Encoding of conditioned fear in central amygdala inhibitory circuits. Nature. Nature Publishing Group; 2010 Nov;468(7321):277–282.
13. Yao Z, Liu H, Xie F, Fischer S, Adkins RS, Aldridge AI, Ament SA, Bartlett A, Behrens MM, Van den Berge K, Bertagnolli D, de Bézieux HR, Biancalani T, Booeshaghi AS, Bravo HC, Casper T, Colantuoni C, Crabtree J, Creasy H, Crichton K, Crow M, Dee N, Dougherty EL, Doyle WI, Dudoit S, Fang R, Felix V, Fong O, Giglio M, Goldy J, Hawrylycz M, Herb BR, Hertzano R, Hou X, Hu Q, Kancherla J, Kroll M, Lathia K, Li YE, Lucero JD, Luo C, Mahurkar A, McMillen D, Nadaf NM, Nery JR, Nguyen TN, Niu SY, Ntranos V, Orvis J, Osteen JK, Pham T, Pinto-Duarte A, Poirion O, Preissl S, Purdom E, Rimorin C, Risso D, Rivkin AC, Smith K, Street K, Sulc J, Svensson V, Tieu M, Torkelson A, Tung H, Vaishnav ED, Vanderburg CR, van Velthoven C, Wang X, White OR, Huang ZJ, Kharchenko PV, Pachter L, Ngai J, Regev A, Tasic B, Welch JD, Gillis J, Macosko EZ, Ren B, Ecker JR,

Zeng H, Mukamel EA. A transcriptomic and epigenomic cell atlas of the mouse primary motor cortex. Nature. 2021;598(7879):103–110. PMCID: PMC8494649

14. Bakken TE, Jorstad NL, Hu Q, Lake BB, Tian W, Kalmbach BE, Crow M, Hodge RD, Krienen FM, Sorensen SA, Eggermont J, Yao Z, Aevermann BD, Aldridge AI, Bartlett A, Bertagnolli D, Casper T, Castanon RG, Crichton K, Daigle TL, Dalley R, Dee N, Dembrow N, Diep D, Ding SL, Dong W, Fang R, Fischer S, Goldman M, Goldy J, Graybuck LT, Herb BR, Hou X, Kancherla J, Kroll M, Lathia K, van Lew B, Li YE, Liu CS, Liu H, Lucero JD, Mahurkar A, McMillen D, Miller JA, Moussa M, Nery JR, Nicovich PR, Niu SY, Orvis J, Osteen JK, Owen S, Palmer CR, Pham T, Plongthongkum N, Poirion O, Reed NM, Rimorin C, Rivkin A, Romanow WJ, Sedeño-Cortés AE, Siletti K, Somasundaram S, Sulc J, Tieu M, Torkelson A, Tung H, Wang X, Xie F, Yanny AM, Zhang R, Ament SA, Behrens MM, Bravo HC, Chun J, Dobin A, Gillis J, Hertzano R, Hof PR, Höllt T, Horwitz GD, Keene CD, Kharchenko PV, Ko AL, Lelieveldt BP, Luo C, Mukamel EA, Pinto-Duarte A, Preissl S, Regev A, Ren B, Scheuermann RH, Smith K, Spain WJ, White OR, Koch C, Hawrylycz M, Tasic B, Macosko EZ, McCarroll SA, Ting JT, Zeng H, Zhang K, Feng G, Ecker JR, Linnarsson S, Lein ES. Comparative cellular analysis of motor cortex in human, marmoset and mouse. Nature. 2021;598(7879):111–119. PMCID: PMC8494640
15. Scala F, Kobak D, Bernabucci M, Bernaerts Y, Cadwell CR, Castro JR, Hartmanis L, Jiang X, Laturnus S, Miranda E, Mulherkar S, Tan ZH, Yao Z, Zeng H, Sandberg R, Berens P, Tolias AS. Phenotypic variation of transcriptomic cell types in mouse motor cortex. Nature. 2021;598(7879):144–150. PMCID: PMC8113357
16. Booeshaghi AS, Yao Z, van Velthoven C, Smith K, Tasic B, Zeng H, Pachter L. Isoform cell-type specificity in the mouse primary motor cortex. Nature. 2021;598(7879):195–199. PMCID: PMC8494650
17. Kozareva V, Martin C, Osorno T, Rudolph S, Guo C, Vanderburg C, Nadaf N, Regev A, Regehr WG, Macosko E. Author Correction: A transcriptomic atlas of mouse cerebellar cortex comprehensively defines cell types. Nature. 2022;602(7896):E21. PMCID: PMC8828463
18. Bhaduri A, Sandoval-Espinosa C, Otero-Garcia M, Oh I, Yin R, Eze UC, Nowakowski TJ, Kriegstein AR. An atlas of cortical arealization identifies dynamic molecular signatures. Nature. 2021;598(7879):200–204. PMCID: PMC8494648
19. Berg J, Sorensen SA, Ting JT, Miller JA, Chartrand T, Buchin A, Bakken TE, Budzillo A, Dee N, Ding SL, Gouwens NW, Hodge RD, Kalmbach B, Lee C, Lee BR, Alfiler L, Baker K, Barkan E, Beller A, Berry K, Bertagnolli D, Bickley K, Bomben J, Braun T, Brouner K, Casper T, Chong P, Crichton K, Dalley R, de Frates R, Desta T, Lee SD, D'Orazi F, Dotson N, Egdorf T, Enstrom R, Farrell C, Feng D, Fong O, Furdan S, Galakhova AA, Gamlin C, Gary A, Glandon A, Goldy J, Gorham M, Goriounova NA, Gratiy S, Graybuck L, Gu H, Hadley K, Hansen N, Heistek TS, Henry AM, Heyer DB, Hill D, Hill C, Hupp M, Jarsky T, Kebede S, Keene L, Kim L, Kim MH, Kroll M, Latimer C, Levi BP, Link KE, Mallory M, Mann R, Marshall D, Maxwell M, McGraw M, McMillen D, Melief E, Mertens EJ, Mezei L, Mihut N, Mok S, Molnar G, Mukora A, Ng L, Ngo K, Nicovich PR, Nyhus J, Olah G, Oldre A, Omstead V, Ozsvar A, Park D, Peng H, Pham T, Pom CA, Potekhina L, Rajanbabu R, Ransford S, Reid D, Rimorin C, Ruiz A, Sandman D, Sulc J, Sunkin SM, Szafer A, Szemenyei V, Thomsen ER, Tieu M, Torkelson A, Trinh J, Tung H, Wakeman W, Waleboer F, Ward K, Wilbers R, Williams G, Yao Z, Yoon JG, Anastassiou C, Arkhipov A, Barzo P, Bernard A, Cobbs C, de Witt Hamer PC, Ellenbogen RG, Esposito L, Ferreira M, Gwinn RP, Hawrylycz MJ, Hof PR, Idema S, Jones AR, Keene CD, Ko AL, Murphy GJ, Ng L, Ojemann JG, Patel AP, Phillips JW, Silbergeld DL, Smith K, Tasic B, Yuste R, Segev I, de Kock CPJ, Mansvelder HD, Tamas G, Zeng H, Koch C, Lein ES. Author Correction: Human neocortical expansion involves glutamatergic neuron diversification. Nature. 2022;601(7893):E12. PMCID: PMC8770134

20. Di Bella DJ, Habibi E, Stickels RR, Scalia G, Brown J, Yadollahpour P, Yang SM, Abbate C, Biancalani T, Macosko EZ, Chen F, Regev A, Arlotta P. Molecular Logic of Cellular Diversification in the Mouse Cerebral Cortex. Nature. 2021 Jul;595(7868):554–559. PMCID: PMC9006333
21. Ziffra RS, Kim CN, Ross JM, Wilfert A, Turner TN, Haeussler M, Casella AM, Przytycki PF, Keough KC, Shin D, Bogdanoff D, Kreimer A, Pollard KS, Ament SA, Eichler EE, Ahituv N, Nowakowski TJ. Single-cell epigenomics reveals mechanisms of human cortical development. Nature. 2021;598(7879):205–213. PMCID: PMC8494642
22. Zhang Z, Zhou J, Tan P, Pang Y, Rivkin AC, Kirchgessner MA, Williams E, Lee CT, Liu H, Franklin AD, Miyazaki PA, Bartlett A, Aldridge AI, Vu M, Boggeman L, Fitzpatrick C, Nery JR, Castanon RG, Rashid M, Jacobs MW, Ito-Cole T, O'Connor C, Pinto-Duartec A, Dominguez B, Smith JB, Niu SY, Lee KF, Jin X, Mukamel EA, Behrens MM, Ecker JR, Callaway EM. Epigenomic diversity of cortical projection neurons in the mouse brain. Nature. 2021;598(7879):167–173. PMCID: PMC8494636
23. Li YE, Preissl S, Hou X, Zhang Z, Zhang K, Qiu Y, Poirion OB, Li B, Chiou J, Liu H, Pinto-Duarte A, Kubo N, Yang X, Fang R, Wang X, Han JY, Lucero J, Yan Y, Miller M, Kuan S, Gorkin D, Gaulton KJ, Shen Y, Nunn M, Mukamel EA, Behrens MM, Ecker JR, Ren B. An atlas of gene regulatory elements in adult mouse cerebrum. Nature. 2021;598(7879):129–136. PMCID: PMC8494637
24. Liu H, Zhou J, Tian W, Luo C, Bartlett A, Aldridge A, Lucero J, Osteen JK, Nery JR, Chen H, Rivkin A, Castanon RG, Clock B, Li YE, Hou X, Poirion OB, Preissl S, Pinto-Duarte A, O'Connor C, Boggeman L, Fitzpatrick C, Nunn M, Mukamel EA, Zhang Z, Callaway EM, Ren B, Dixon JR, Behrens MM, Ecker JR. DNA methylation atlas of the mouse brain at single-cell resolution. Nature. 2021;598(7879):120–128. PMCID: PMC8494641
25. Domcke S, Hill AJ, Daza RM, Cao J, O'Day DR, Pliner HA, Aldinger KA, Pokholok D, Zhang F, Milbank JH, Zager MA, Glass IA, Steemers FJ, Doherty D, Trapnell C, Cusanovich DA, Shendure J. A human cell atlas of fetal chromatin accessibility. Science. 2020 Nov 13;370(6518):eaba7612. PMCID: PMC7785298
26. Zhang K, Hocker JD, Miller M, Hou X, Chiou J, Poirion OB, Qiu Y, Li YE, Gaulton KJ, Wang A, Preissl S, Ren B. A single-cell atlas of chromatin accessibility in the human genome. Cell. 2021 Nov 24;184(24):5985-6001.e19. PMCID: PMC8664161
27. Moore JE, Purcaro MJ, Pratt HE, Epstein CB, Shoresh N, Adrian J, Kawli T, Davis CA, Dobin A, Kaul R, Halow J, Van Nostrand EL, Freese P, Gorkin DU, Shen Y, He Y, Mackiewicz M, Pauli-Behn F, Williams BA, Mortazavi A, Keller CA, Zhang XO, Elhajjajy SI, Huey J, Dickel DE, Snetkova V, Wei X, Wang X, Rivera-Mulia JC, Rozowsky J, Zhang J, Chhetri SB, Zhang J, Victorsen A, White KP, Visel A, Yeo GW, Burge CB, Lécuyer E, Gilbert DM, Dekker J, Rinn J, Mendenhall EM, Ecker JR, Kellis M, Klein RJ, Noble WS, Kundaje A, Guigó R, Farnham PJ, Cherry JM, Myers RM, Ren B, Graveley BR, Gerstein MB, Pennacchio LA, Snyder MP, Bernstein BE, Wold B, Hardison RC, Gingeras TR, Stamatoyannopoulos JA, Weng Z. Expanded encyclopaedias of DNA elements in the human and mouse genomes. Nature. 2020;583(7818):699–710. PMCID: PMC7410828
28. Shlyueva D, Stampfel G, Stark A. Transcriptional enhancers: from properties to genome-wide predictions. Nature Reviews Genetics. 2014 Apr;15(4):272–286.
29. Buenrostro JD, Wu B, Litzenburger UM, Ruff D, Gonzales ML, Snyder MP, Chang HY, Greenleaf WJ. Single-cell chromatin accessibility reveals principles of regulatory variation. Nature. 2015 Jul 23;523(7561):486–490. PMCID: PMC4685948
30. Cusanovich DA, Hill AJ, Aghamirzaie D, Daza RM, Pliner HA, Berletch JB, Filippova GN, Huang X, Christiansen L, DeWitt WS, Lee C, Regalado SG, Read DF, Steemers FJ, Disteche CM, Trapnell C, Shendure J. A Single-Cell Atlas of In Vivo Mammalian Chromatin Accessibility. Cell. Elsevier; 2018 Aug 23;174(5):1309-1324.e18. PMID: 30078704
31. Zhang F, Lupski JR. Non-coding genetic variants in human disease. Hum Mol Genet. 2015

Oct 15;24(R1):R102–R110. PMCID: PMC4572001
32. Srinivasan C, Phan BN, Lawler AJ, Ramamurthy E, Kleyman M, Brown AR, Kaplow IM, Wirthlin ME, Pfenning AR. Addiction-Associated Genetic Variants Implicate Brain Cell Type- and Region-Specific Cis-Regulatory Elements in Addiction Neurobiology. J Neurosci. 2021 Oct 27;41(43):9008–9030. PMCID: PMC8549541
33. Tran MN, Maynard KR, Spangler A, Huuki LA, Montgomery KD, Sadashivaiah V, Tippani M, Barry BK, Hancock DB, Hicks SC, Kleinman JE, Hyde TM, Collado-Torres L, Jaffe AE, Martinowich K. Single-nucleus transcriptome analysis reveals cell-type-specific molecular signatures across reward circuitry in the human brain. Neuron. Elsevier; 2021 Oct 6;109(19):3088-3103.e5. PMID: 34582785
34. Chen R, Blosser TR, Djekidel MN, Hao J, Bhattacherjee A, Chen W, Tuesta LM, Zhuang X, Zhang Y. Decoding molecular and cellular heterogeneity of mouse nucleus accumbens. Nat Neurosci. 2021 Dec;24(12):1757–1771. PMCID: PMC8639815
35. He J, Kleyman M, Chen J, Alikaya A, Rothenhoefer KM, Ozturk BE, Wirthlin M, Bostan AC, Fish K, Byrne LC, Pfenning AR, Stauffer WR. Transcriptional and anatomical diversity of medium spiny neurons in the primate striatum. Current Biology. Elsevier; 2021 Dec 20;31(24):5473-5486.e6. PMID: 34727523
36. Phillips RA, Tuscher JJ, Black SL, Andraka E, Fitzgerald ND, Ianov L, Day JJ. An atlas of transcriptionally defined cell populations in the rat ventral tegmental area. Cell Reports [Internet]. Elsevier; 2022 Apr 5 [cited 2022 Aug 4];39(1). Available from: https://www.cell.com/cell-reports/abstract/S2211-1247(22)00364-3 PMID: 35385745
37. Avey D, Sankararaman S, Yim AKY, Barve R, Milbrandt J, Mitra RD. Single-Cell RNA-Seq Uncovers a Robust Transcriptional Response to Morphine by Glia. Cell Rep. 2018 Sep 25;24(13):3619-3629.e4. PMCID: PMC6357782
38. Savell KE, Tuscher JJ, Zipperly ME, Duke CG, Phillips RA, Bauman AJ, Thukral S, Sultan FA, Goska NA, Ianov L, Day JJ. A dopamine-induced gene expression signature regulates neuronal function and cocaine response. Science Advances. American Association for the Advancement of Science; 2020 Jun 1;6(26):eaba4221.
39. Carrette LLG, Guglielmo G de, Kallupi M, Maturin L, Brennan M, Boomhower B, Conlisk D, Sedighim S, Tieu L, Fannon MJ, Velarde N, Martinez AR, Kononoff J, Kimbrough A, Simpson S, Smith LC, Shankar K, Ramirez FJ, Chitre AS, Lin B, Polesskaya O, Woods LCS, Palmer AA, George O. The Cocaine and Oxycodone Biobanks, Two Repositories from Genetically Diverse and Behaviorally Characterized Rats for the Study of Addiction. eNeuro [Internet]. Society for Neuroscience; 2021 May 1 [cited 2021 Aug 2];8(3). Available from: https://www.eneuro.org/content/8/3/ENEURO.0033-21.2021 PMID: 33875455
40. Chen BT, Yau HJ, Hatch C, Kusumoto-Yoshida I, Cho SL, Hopf FW, Bonci A. Rescuing cocaine-induced prefrontal cortex hypoactivity prevents compulsive cocaine seeking. Nature. Nature Publishing Group; 2013 Apr;496(7445):359–362.
41. Cohen A, Koob GF, George O. Robust Escalation of Nicotine Intake with Extended Access to Nicotine Self-Administration and Intermittent Periods of Abstinence. Neuropsychopharmacology. Nature Publishing Group; 2012 Aug;37(9):2153–2160.
42. Koob GF, Buck CL, Cohen A, Edwards S, Park PE, Schlosburg JE, Schmeichel B, Vendruscolo LF, Wade CL, Whitfield TW, George O. Addiction as a Stress Surfeit Disorder. Neuropharmacology. 2014 Jan;76(0 0):10.1016/j.neuropharm.2013.05.024. PMCID: PMC3830720
43. Solberg Woods LC, Palmer AA. Using Heterogeneous Stocks for Fine-Mapping Genetically Complex Traits. Methods Mol Biol. 2019;2018:233–247. PMCID: PMC9121584
44. Hansen C, Spuhler K. Development of the National Institutes of Health genetically heterogeneous rat stock. Alcohol Clin Exp Res. 1984 Oct;8(5):477–479. PMID: 6391259
45. Saar K, Beck A, Bihoreau MT, Birney E, Brocklebank D, Chen Y, Cuppen E, Demonchy S, Flicek P, Foglio M, Fujiyama A, Gut IG, Gauguier D, Guigo R, Guryev V, Heinig M, Hummel

O, Jahn N, Klages S, Kren V, Kuhl H, Kuramoto T, Kuroki Y, Lechner D, Lee YA, Lopez-Bigas N, Lathrop GM, Mashimo T, Kube M, Mott R, Patone G, Perrier-Cornet JA, Platzer M, Pravenec M, Reinhardt R, Sakaki Y, Schilhabel M, Schulz H, Serikawa T, Shikhagaie M, Tatsumoto S, Taudien S, Toyoda A, Voigt B, Zelenika D, Zimdahl H, Hubner N. SNP and haplotype mapping for genetic analysis in the Rat. Nat Genet. 2008 May;40(5):560–566. PMCID: PMC5915293

46. Baud A, Hermsen R, Guryev V, Stridh P, Graham D, McBride MW, Foroud T, Calderari S, Diez M, Ockinger J, Beyeen AD, Gillett A, Abdelmagid N, Guerreiro-Cacais AO, Jagodic M, Tuncel J, Norin U, Beattie E, Huynh N, Miller WH, Koller DL, Alam I, Falak S, Osborne-Pellegrin M, Martinez-Membrives E, Canete T, Blazquez G, Vicens-Costa E, Mont-Cardona C, Diaz-Moran S, Tobena A, Hummel O, Zelenika D, Saar K, Patone G, Bauerfeind A, Bihoreau MT, Heinig M, Lee YA, Rintisch C, Schulz H, Wheeler DA, Worley KC, Muzny DM, Gibbs RA, Lathrop M, Lansu N, Toonen P, Ruzius FP, de Bruijn E, Hauser H, Adams DJ, Keane T, Atanur SS, Aitman TJ, Flicek P, Malinauskas T, Jones EY, Ekman D, Lopez-Aumatell R, Dominiczak AF, Johannesson M, Holmdahl R, Olsson T, Gauguier D, Hubner N, Fernandez-Teruel A, Cuppen E, Mott R, Flint J. Combined sequence-based and genetic mapping analysis of complex traits in outbred rats. Nat Genet. 2013 Jul;45(7):10.1038/ng.2644. PMCID: PMC3821058
47. Carrette LLG, Corral C, Boomhower B, Brennan M, Crook C, Ortez C, Shankar K, Simpson S, Maturin L, Solberg Woods LC, Palmer AA, de Guglielmo G, George O. Leptin Protects Against the Development and Expression of Cocaine Addiction-Like Behavior in Heterogeneous Stock Rats. Front Behav Neurosci. 2022 Mar 3;16:832899. PMCID: PMC8934439
48. Characterization of cocaine addiction-like behavior in heterogeneous stock rats | bioRxiv [Internet]. [cited 2022 Jun 9]. Available from: https://www.biorxiv.org/content/10.1101/2021.07.22.453410v2
49. Sedighim S, Carrette LL, Venniro M, Shaham Y, de Guglielmo G, George O. Individual differences in addiction-like behaviors and choice between cocaine versus food in Heterogeneous Stock rats. Psychopharmacology (Berl). 2021 Dec;238(12):3423–3433. PMCID: PMC8889911
50. George O, Mandyam CD, Wee S, Koob GF. Extended Access to Cocaine Self-Administration Produces Long-Lasting Prefrontal Cortex-Dependent Working Memory Impairments. Neuropsychopharmacology. 2008 Sep;33(10):2474–2482. PMCID: PMC2760333
51. Belin D, Balado E, Piazza PV, Deroche-Gamonet V. Pattern of intake and drug craving predict the development of cocaine addiction-like behavior in rats. Biol Psychiatry. 2009 May 15;65(10):863–868. PMID: 18639867
52. Deroche-Gamonet V, Belin D, Piazza PV. Evidence for addiction-like behavior in the rat. Science. 2004 Aug 13;305(5686):1014–1017. PMID: 15310906
53. Belin D, Deroche-Gamonet V. Responses to Novelty and Vulnerability to Cocaine Addiction: Contribution of a Multi-Symptomatic Animal Model. Cold Spring Harb Perspect Med. Cold Spring Harbor Laboratory Press; 2012 Nov 1;2(11):a011940. PMID: 23125204
54. Koob GF, Volkow ND. Neurobiology of addiction: a neurocircuitry analysis. Lancet Psychiatry. 2016 Aug;3(8):760–773. PMCID: PMC6135092
55. Yu B, Zhang Q, Lin L, Zhou X, Ma W, Wen S, Li C, Wang W, Wu Q, Wang X, Li XM. Molecular and cellular evolution of the amygdala across species analyzed by single-nucleus transcriptome profiling. Cell Discov. Nature Publishing Group; 2023 Feb 14;9(1):1–22.
56. Stuart T, Butler A, Hoffman P, Hafemeister C, Papalexi E, Mauck WM, Hao Y, Stoeckius M, Smibert P, Satija R. Comprehensive integration of single-cell data. Cell. 2019 Jun 13;177(7):1888-1902.e21. PMCID: PMC6687398
57. Stuart T, Srivastava A, Madad S, Lareau CA, Satija R. Single-cell chromatin state analysis

with Signac. Nat Methods. Nature Publishing Group; 2021 Nov;18(11):1333–1341.
58. Butler A, Hoffman P, Smibert P, Papalexi E, Satija R. Integrating single-cell transcriptomic data across different conditions, technologies, and species. Nature Biotechnology. Nature Publishing Group; 2018 May;36(5):411–420.
59. Zeisel A, Hochgerner H, Lönnerberg P, Johnsson A, Memic F, van der Zwan J, Häring M, Braun E, Borm LE, La Manno G, Codeluppi S, Furlan A, Lee K, Skene N, Harris KD, Hjerling-Leffler J, Arenas E, Ernfors P, Marklund U, Linnarsson S. Molecular Architecture of the Mouse Nervous System. Cell. 2018 Aug 9;174(4):999-1014.e22. PMCID: PMC6086934
60. Saunders A, Macosko E, Wysoker A, Goldman M, Krienen F, de Rivera H, Bien E, Baum M, Wang S, Goeva A, Nemesh J, Kamitaki N, Brumbaugh S, Kulp D, McCarroll SA. Molecular Diversity and Specializations among the Cells of the Adult Mouse Brain. Cell. 2018 Aug 9;174(4):1015-1030.e16. PMCID: PMC6447408
61. Tasic B, Yao Z, Graybuck LT, Smith KA, Nguyen TN, Bertagnolli D, Goldy J, Garren E, Economo MN, Viswanathan S, Penn O, Bakken T, Menon V, Miller J, Fong O, Hirokawa KE, Lathia K, Rimorin christine, Tieu M, Larsen R, casper T, Barkan E, Kroll M, Parry S, Shapovalova NV, Hirschstein D, Pendergraft J, Sullivan HA, Kim TK, Szafer A, Dee N, Groblewski P, Wickersham ian, cetin A, Harris JA, Levi BP, Sunkin SM, Madisen L, Daigle TL, Looger L, Bernard A, Phillips J, Lein E, Hawrylycz M, Svoboda K, Jones AR, Koch christof, Zeng H. Shared and distinct transcriptomic cell types across neocortical areas. Nature. 2018 Nov;563(7729):72–78. PMCID: PMC6456269
62. Yao Z, van Velthoven CTJ, Nguyen TN, Goldy J, Sedeno-Cortes AE, Baftizadeh F, Bertagnolli D, Casper T, Chiang M, Crichton K, Ding SL, Fong O, Garren E, Glandon A, Gouwens NW, Gray J, Graybuck LT, Hawrylycz MJ, Hirschstein D, Kroll M, Lathia K, Lee C, Levi B, McMillen D, Mok S, Pham T, Ren Q, Rimorin C, Shapovalova N, Sulc J, Sunkin SM, Tieu M, Torkelson A, Tung H, Ward K, Dee N, Smith KA, Tasic B, Zeng H. A taxonomy of transcriptomic cell types across the isocortex and hippocampal formation. Cell. 2021 Jun 10;184(12):3222-3241.e26. PMCID: PMC8195859
63. BRAIN Initiative Cell Census Network (BICCN). A multimodal cell census and atlas of the mammalian primary motor cortex. Nature. 2021 Oct;598(7879):86–102. PMCID: PMC8494634
64. O'Leary TP, Sullivan KE, Wang L, Clements J, Lemire AL, Cembrowski MS. Extensive and spatially variable within-cell-type heterogeneity across the basolateral amygdala. eLife. 9:e59003. PMCID: PMC7486123
65. Beyeler A, Dabrowska J. Neuronal diversity of the amygdala and the bed nucleus of the stria terminalis. Handb Behav Neurosci. 2020;26:63–100. PMCID: PMC7423190
66. Leek JT, Scharpf RB, Bravo HC, Simcha D, Langmead B, Johnson WE, Geman D, Baggerly K, Irizarry RA. Tackling the widespread and critical impact of batch effects in high-throughput data. Nat Rev Genet. 2010 Oct;11(10):10.1038/nrg2825. PMCID: PMC3880143
67. Tran HTN, Ang KS, Chevrier M, Zhang X, Lee NYS, Goh M, Chen J. A benchmark of batch-effect correction methods for single-cell RNA sequencing data. Genome Biology. 2020 Jan 16;21(1):12.
68. Banovich NE, Lan X, McVicker G, Geijn B van de, Degner JF, Blischak JD, Roux J, Pritchard JK, Gilad Y. Methylation QTLs Are Associated with Coordinated Changes in Transcription Factor Binding, Histone Modifications, and Gene Expression Levels. PLOS Genetics. Public Library of Science; 2014 Sep 18;10(9):e1004663.
69. Degner JF, Pai AA, Pique-Regi R, Veyrieras JB, Gaffney DJ, Pickrell JK, De Leon S, Michelini K, Lewellen N, Crawford GE, Stephens M, Gilad Y, Pritchard JK. DNase I sensitivity QTLs are a major determinant of human expression variation. Nature. Nature Publishing Group; 2012 Feb;482(7385):390–394.
70. Munro D, Wang T, Chitre AS, Polesskaya O, Ehsan N, Gao J, Gusev A, Woods LCS, Saba LM, Chen H, Palmer AA, Mohammadi P. The regulatory landscape of multiple brain regions

in outbred heterogeneous stock rats [Internet]. bioRxiv; 2022 [cited 2022 Aug 17]. p. 2022.04.07.487560. Available from: https://www.biorxiv.org/content/10.1101/2022.04.07.487560v1

71. Liu M, Tan X, Liu E, Hang Z, Song R, Mu S, Han W, Yue Q, Sun J. Inactivation of the Lateral Hypothalamus Attenuates Methamphetamine-Induced Conditioned Place Preference through Regulation of Kcnq3 Expression. Int J Mol Sci. 2022 Jun 30;23(13):7305. PMCID: PMC9266452
72. Tsuboi D, Otsuka T, Shimomura T, Faruk MO, Yamahashi Y, Amano M, Funahashi Y, Kuroda K, Nishioka T, Kobayashi K, Sano H, Nagai T, Yamada K, Tzingounis AV, Nambu A, Kubo Y, Kawaguchi Y, Kaibuchi K. Dopamine drives neuronal excitability via KCNQ channel phosphorylation for reward behavior. Cell Reports [Internet]. Elsevier; 2022 Sep 6 [cited 2023 Apr 21];40(10). Available from: https://www.cell.com/cell-reports/abstract/S2211-1247(22)01133-0 PMID: 36070693
73. Hansen HH, Andreasen JT, Weikop P, Mirza N, Scheel-Krüger J, Mikkelsen JD. The neuronal KCNQ channel opener retigabine inhibits locomotor activity and reduces forebrain excitatory responses to the psychostimulants cocaine, methylphenidate and phencyclidine. Eur J Pharmacol. 2007 Sep 10;570(1–3):77–88. PMID: 17628530
74. Cruz B, Vozella V, Carper BA, Xu JC, Kirson D, Hirsch S, Nolen T, Bradley L, Fain K, Crawford M, Kosten TR, Zorrilla EP, Roberto M. FKBP5 inhibitors modulate alcohol drinking and trauma-related behaviors in a model of comorbid post-traumatic stress and alcohol use disorder. Neuropsychopharmacol. Nature Publishing Group; 2022 Nov 18;1–11.
75. Levran O, Peles E, Randesi M, Li Y, Rotrosen J, Ott J, Adelson M, Kreek MJ. Stress-related genes and heroin addiction: a role for a functional FKBP5 haplotype. Psychoneuroendocrinology. 2014 Jul;45:67–76. PMCID: PMC4316666
76. Heller EA, Kaska S, Fallon B, Ferguson D, Kennedy PJ, Neve RL, Nestler EJ, Mazei-Robison MS. Morphine and cocaine increase serum- and glucocorticoid-inducible kinase 1 activity in the ventral tegmental area. J Neurochem. 2015 Jan;132(2):243–253. PMCID: PMC4302038
77. Mohammadi P, Castel SE, Brown AA, Lappalainen T. Quantifying the regulatory effect size of cis-acting genetic variation using allelic fold change. Genome Res. 2017 Nov 1;27(11):1872–1884.
78. Subramanian A, Tamayo P, Mootha VK, Mukherjee S, Ebert BL, Gillette MA, Paulovich A, Pomeroy SL, Golub TR, Lander ES, Mesirov JP. Gene set enrichment analysis: A knowledge-based approach for interpreting genome-wide expression profiles. Proc Natl Acad Sci U S A. 2005 Oct 25;102(43):15545–15550. PMCID: PMC1239896
79. Mootha VK, Lindgren CM, Eriksson KF, Subramanian A, Sihag S, Lehar J, Puigserver P, Carlsson E, Ridderstråle M, Laurila E, Houstis N, Daly MJ, Patterson N, Mesirov JP, Golub TR, Tamayo P, Spiegelman B, Lander ES, Hirschhorn JN, Altshuler D, Groop LC. PGC-1α-responsive genes involved in oxidative phosphorylation are coordinately downregulated in human diabetes. Nat Genet. Nature Publishing Group; 2003 Jul;34(3):267–273.
80. Kasischke KA, Vishwasrao HD, Fisher PJ, Zipfel WR, Webb WW. Neural activity triggers neuronal oxidative metabolism followed by astrocytic glycolysis. Science. 2004 Jul 2;305(5680):99–103. PMID: 15232110
81. Attwell D, Laughlin SB. An energy budget for signaling in the grey matter of the brain. J Cereb Blood Flow Metab. 2001 Oct;21(10):1133–1145. PMID: 11598490
82. Distler MG, Plant LD, Sokoloff G, Hawk AJ, Aneas I, Wuenschell GE, Termini J, Meredith SC, Nobrega MA, Palmer AA. Glyoxalase 1 increases anxiety by reducing GABAA receptor agonist methylglyoxal. J Clin Invest. 2012 Jun 1;122(6):2306–2315. PMCID: PMC3366407
83. Perez CL, Barkley-Levenson AM, Dick BL, Glatt PF, Martinez Y, Siegel D, Momper JD, Palmer AA, Cohen SM. A Metal-Binding Pharmacophore Library Yields the Discovery of a Glyoxalase 1 Inhibitor. J Med Chem. 2019 Feb 14;62(3):1609–1625. PMCID: PMC6467756

84. Delaney AJ, Crane JW, Holmes NM, Fam J, Westbrook RF. Baclofen acts in the central amygdala to reduce synaptic transmission and impair context fear conditioning. Sci Rep. 2018 Jul 2;8:9908. PMCID: PMC6028433
85. Li C, Pleil KE, Stamatakis AM, Busan S, Vong L, Lowell BB, Stuber GD, Kash TL. Presynaptic inhibition of GABA release in the BNST by kappa opioid receptor signaling. Biol Psychiatry. 2012 Apr 15;71(8):725–732. PMCID: PMC3314138
86. de Guglielmo G, Conlisk DE, Barkley-Levenson AM, Palmer AA, George O. Inhibition of Glyoxalase 1 reduces alcohol self-administration in dependent and nondependent rats. Pharmacol Biochem Behav. 2018 Apr;167:36–41. PMCID: PMC5866249
87. Zhang Y, Liu T, Meyer CA, Eeckhoute J, Johnson DS, Bernstein BE, Nusbaum C, Myers RM, Brown M, Li W, Liu XS. Model-based Analysis of ChIP-Seq (MACS). Genome Biology. 2008 Sep 17;9(9):R137.
88. Robinson MD, McCarthy DJ, Smyth GK. edgeR: a Bioconductor package for differential expression analysis of digital gene expression data. Bioinformatics. 2010 Jan 1;26(1):139–140. PMCID: PMC2796818
89. Love MI, Huber W, Anders S. Moderated estimation of fold change and dispersion for RNA-seq data with DESeq2. Genome Biology. 2014 Dec 5;15(12):550.
90. Schep AN, Wu B, Buenrostro JD, Greenleaf WJ. chromVAR: inferring transcription-factor-associated accessibility from single-cell epigenomic data. Nature Methods. Nature Publishing Group; 2017 Oct;14(10):975–978.
91. Matsuda T, Irie T, Katsurabayashi S, Hayashi Y, Nagai T, Hamazaki N, Adefuin AMD, Miura F, Ito T, Kimura H, Shirahige K, Takeda T, Iwasaki K, Imamura T, Nakashima K. Pioneer Factor NeuroD1 Rearranges Transcriptional and Epigenetic Profiles to Execute Microglia-Neuron Conversion. Neuron. Elsevier; 2019 Feb 6;101(3):472-485.e7. PMID: 30638745
92. Glahs A, Zinzen RP. Putting chromatin in its place: the pioneer factor NeuroD1 modulates chromatin state to drive cell fate decisions. EMBO J. 2016 Jan 4;35(1):1–3. PMCID: PMC4718001
93. Cruz FC, Rubio FJ, Hope BT. Using c-fos to study neuronal ensembles in corticostriatal circuitry of addiction. Brain Res. 2015 Dec 2;1628(0 0):157–173. PMCID: PMC4427550
94. Zhang Y, Crofton EJ, Li D, Lobo MK, Fan X, Nestler EJ, Green TA. Overexpression of DeltaFosB in nucleus accumbens mimics the protective addiction phenotype, but not the protective depression phenotype of environmental enrichment. Frontiers in Behavioral Neuroscience [Internet]. 2014 [cited 2022 Aug 4];8. Available from: https://www.frontiersin.org/articles/10.3389/fnbeh.2014.00297
95. Bali P, Kenny PJ. Transcriptional mechanisms of drug addiction. Dialogues Clin Neurosci. 2019 Dec;21(4):379–387. PMCID: PMC6952748
96. Walker DM, Cates HM, Loh YHE, Purushothaman I, Ramakrishnan A, Cahill KM, Lardner CK, Godino A, Kronman HG, Rabkin J, Lorsch ZS, Mews P, Doyle MA, Feng J, Labonté B, Koo JW, Bagot RC, Logan RW, Seney ML, Calipari ES, Shen L, Nestler EJ. Cocaine self-administration alters transcriptome-wide responses in the brain's reward circuitry. Biol Psychiatry. 2018 Dec 15;84(12):867–880. PMCID: PMC6202276
97. Nestler EJ, Barrot M, Self DW. ΔFosB: A sustained molecular switch for addiction. Proceedings of the National Academy of Sciences. 2001 Sep 25;98(20):11042–11046.
98. Hope BT, Nye HE, Kelz MB, Self DW, Iadarola MJ, Nakabeppu Y, Duman RS, Nestler EJ. Induction of a long-lasting AP-1 complex composed of altered Fos-like proteins in brain by chronic cocaine and other chronic treatments. Neuron. Elsevier; 1994 Nov 1;13(5):1235–1244. PMID: 7946359
99. Nye HE, Nestler EJ. Induction of chronic Fos-related antigens in rat brain by chronic morphine administration. Mol Pharmacol. American Society for Pharmacology and Experimental Therapeutics; 1996 Apr 1;49(4):636–645. PMID: 8609891
100. Nye HE, Hope BT, Kelz MB, Iadarola M, Nestler EJ. Pharmacological studies of the

regulation of chronic FOS-related antigen induction by cocaine in the striatum and nucleus accumbens. J Pharmacol Exp Ther. American Society for Pharmacology and Experimental Therapeutics; 1995 Dec 1;275(3):1671–1680. PMID: 8531143

101. Moratalla R, Elibol B, Vallejo M, Graybiel AM. Network-Level Changes in Expression of Inducible Fos–Jun Proteins in the Striatum during Chronic Cocaine Treatment and Withdrawal. Neuron. Elsevier; 1996 Jul 1;17(1):147–156. PMID: 8755486
102. Song L, Zhang Z, Grasfeder LL, Boyle AP, Giresi PG, Lee BK, Sheffield NC, Gräf S, Huss M, Keefe D, Liu Z, London D, McDaniell RM, Shibata Y, Showers KA, Simon JM, Vales T, Wang T, Winter D, Zhang Z, Clarke ND, Birney E, Iyer VR, Crawford GE, Lieb JD, Furey TS. Open chromatin defined by DNaseI and FAIRE identifies regulatory elements that shape cell-type identity. Genome Res. 2011 Oct;21(10):1757–1767. PMCID: PMC3202292
103. Klemm SL, Shipony Z, Greenleaf WJ. Chromatin accessibility and the regulatory epigenome. Nat Rev Genet. Nature Publishing Group; 2019 Apr;20(4):207–220.
104. Cano-Gamez E, Trynka G. From GWAS to Function: Using Functional Genomics to Identify the Mechanisms Underlying Complex Diseases. Front Genet. 2020 May 13;11:424. PMCID: PMC7237642
105. Bulik-Sullivan BK, Loh PR, Finucane HK, Ripke S, Yang J, Patterson N, Daly MJ, Price AL, Neale BM. LD Score regression distinguishes confounding from polygenicity in genome-wide association studies. Nature Genetics. Nature Publishing Group; 2015 Mar;47(3):291–295.
106. Liu M, Jiang Y, Wedow R, Li Y, Brazel DM, Chen F, Datta G, Davila-Velderrain J, McGuire D, Tian C, Zhan X, Choquet H, Docherty AR, Faul JD, Foerster JR, Fritsche LG, Gabrielsen ME, Gordon SD, Haessler J, Hottenga JJ, Huang H, Jang SK, Jansen PR, Ling Y, Mägi R, Matoba N, McMahon G, Mulas A, Orrù V, Palviainen T, Pandit A, Reginsson GW, Skogholt AH, Smith JA, Taylor AE, Turman C, Willemsen G, Young H, Young KA, Zajac GJM, Zhao W, Zhou W, Bjornsdottir G, Boardman JD, Boehnke M, Boomsma DI, Chen C, Cucca F, Davies GE, Eaton CB, Ehringer MA, Esko T, Fiorillo E, Gillespie NA, Gudbjartsson DF, Haller T, Harris KM, Heath AC, Hewitt JK, Hickie IB, Hokanson JE, Hopfer CJ, Hunter DJ, Iacono WG, Johnson EO, Kamatani Y, Kardia SLR, Keller MC, Kellis M, Kooperberg C, Kraft P, Krauter KS, Laakso M, Lind PA, Loukola A, Lutz SM, Madden PAF, Martin NG, McGue M, McQueen MB, Medland SE, Metspalu A, Mohlke KL, Nielsen JB, Okada Y, Peters U, Polderman TJC, Posthuma D, Reiner AP, Rice JP, Rimm E, Rose RJ, Runarsdottir V, Stallings MC, Stančáková A, Stefansson H, Thai KK, Tindle HA, Tyrfingsson T, Wall TL, Weir DR, Weisner C, Whitfield JB, Winsvold BS, Yin J, Zuccolo L, Bierut LJ, Hveem K, Lee JJ, Munafò MR, Saccone NL, Willer CJ, Cornelis MC, David SP, Hinds DA, Jorgenson E, Kaprio J, Stitzel JA, Stefansson K, Thorgeirsson TE, Abecasis G, Liu DJ, Vrieze S. Association studies of up to 1.2 million individuals yield new insights into the genetic etiology of tobacco and alcohol use. Nature Genetics. Nature Publishing Group; 2019 Feb;51(2):237–244.
107. Polimanti R, Walters RK, Johnson EC, McClintick JN, Adkins AE, Adkins DE, Bacanu SA, Bierut LJ, Bigdeli TB, Brown S, Bucholz KK, Copeland WE, Costello EJ, Degenhardt L, Farrer LA, Foroud TM, Fox L, Goate AM, Grucza R, Hack LM, Hancock DB, Hartz SM, Heath AC, Hewitt JK, Hopfer CJ, Johnson EO, Kendler KS, Kranzler HR, Krauter K, Lai D, Madden PAF, Martin NG, Maes HH, Nelson EC, Peterson RE, Porjesz B, Riley BP, Saccone N, Stallings M, Wall TL, Webb BT, Wetherill L, Edenberg HJ, Agrawal A, Gelernter J. Leveraging genome-wide data to investigate differences between opioid use vs. opioid dependence in 41,176 individuals from the Psychiatric Genomics Consortium. Molecular Psychiatry. Nature Publishing Group; 2020 Aug;25(8):1673–1687.
108. Hatoum AS, Johnson EC, Colbert SMC, Polimanti R, Zhou H, Walters RK, Gelernter J, Edenberg HJ, Bogdan R, Agrawal A. The addiction risk factor: A unitary genetic vulnerability characterizes substance use disorders and their associations with common correlates.

Neuropsychopharmacology. 2022 Sep;47(10):1739–1745. PMCID: PMC9372072
109. Wade CL, Vendruscolo LF, Schlosburg JE, Hernandez DO, Koob GF. Compulsive-Like Responding for Opioid Analgesics in Rats with Extended Access. Neuropsychopharmacology. 2015 Jan;40(2):421–428. PMCID: PMC4443956
110. Visscher PM, Yengo L, Cox NJ, Wray NR. Discovery and implications of polygenicity of common diseases. Science. American Association for the Advancement of Science; 2021 Sep 24;373(6562):1468–1473.
111. Zaret KS. Pioneer Transcription Factors Initiating Gene Network Changes. Annu Rev Genet. 2020 Nov 23;54:367–385. PMCID: PMC7900943
112. Chitre AS, Polesskaya O, Holl K, Gao J, Cheng R, Bimschleger H, Martinez AG, George T, Gileta AF, Han W, Horvath A, Hughson A, Ishiwari K, King CP, Lamparelli A, Versaggi CL, Martin C, St. Pierre CL, Tripi JA, Wang T, Chen H, Flagel SB, Meyer P, Richards J, Robinson TE, Palmer AA, Woods LCS. Genome wide association study in 3,173 outbred rats identifies multiple loci for body weight, adiposity, and fasting glucose. Obesity (Silver Spring). 2020 Oct;28(10):1964–1973. PMCID: PMC7511439
113. Stephens DN, King SL, Lambert JJ, Belelli D, Duka T. GABAA receptor subtype involvement in addictive behaviour. Genes Brain Behav. 2017 Jan;16(1):149–184. PMID: 27539865
114. Koob GF, Nestler EJ. The neurobiology of drug addiction. J Neuropsychiatry Clin Neurosci. 1997;9(3):482–497. PMID: 9276849
115. Koob GF. A role for GABA mechanisms in the motivational effects of alcohol. Biochemical Pharmacology. 2004 Oct 15;68(8):1515–1525.
116. Dixon CI, Morris HV, Breen G, Desrivieres S, Jugurnauth S, Steiner RC, Vallada H, Guindalini C, Laranjeira R, Messas G, Rosahl TW, Atack JR, Peden DR, Belelli D, Lambert JJ, King SL, Schumann G, Stephens DN. Cocaine effects on mouse incentive-learning and human addiction are linked to α2 subunit-containing GABAA receptors. Proc Natl Acad Sci U S A. 2010 Feb 2;107(5):2289–2294. PMCID: PMC2836671
117. Augier E, Barbier E, Dulman RS, Licheri V, Augier G, Domi E, Barchiesi R, Farris S, Nätt D, Mayfield RD, Adermark L, Heilig M. A molecular mechanism for choosing alcohol over an alternative reward. Science. American Association for the Advancement of Science; 2018 Jun 22;360(6395):1321–1326.
118. Kallupi M, Wee S, Edwards S, Whitfield TW, Oleata CS, Luu G, Schmeichel BE, Koob GF, Roberto M. Kappa Opioid Receptor-Mediated Dysregulation of GABAergic Transmission in the Central Amygdala in Cocaine Addiction. Biol Psychiatry. 2013 Oct 1;74(7):520–528. PMCID: PMC3773286
119. McMurray KMJ, Ramaker MJ, Barkley-Levenson AM, Sidhu PS, Elkin P, Reddy MK, Guthrie ML, Cook JM, Rawal VH, Arnold LA, Dulawa SC, Palmer AA. Identification of a novel, fast acting GABAergic anti-depressant. Mol Psychiatry. 2018 Feb;23(2):384–391. PMCID: PMC5608625
120. Williams CL, Buchta WC, Riegel AC. CRF-R2 and the Heterosynaptic Regulation of VTA Glutamate during Reinstatement of Cocaine Seeking. J Neurosci. 2014 Jul 30;34(31):10402–10414. PMCID: PMC4115144
121. Bentzley BS, Aston-Jones G. Inhibiting subthalamic nucleus decreases cocaine demand and relapse: Therapeutic potential. Addict Biol. 2017 Jul;22(4):946–957. PMCID: PMC5010790
122. Shinohara F, Kamii H, Minami M, Kaneda K. The Role of Dopaminergic Signaling in the Medial Prefrontal Cortex for the Expression of Cocaine-Induced Conditioned Place Preference in Rats. Biol Pharm Bull. 2017;40(11):1983–1989. PMID: 29093348
123. Mitchell SJ, Maguire EP, Cunningham L, Gunn BG, Linke M, Zechner U, Dixon CI, King SL, Stephens DN, Swinny JD, Belelli D, Lambert JJ. Early-life adversity selectively impairs α2-GABAA receptor expression in the mouse nucleus accumbens and influences the

behavioral effects of cocaine. Neuropharmacology. 2018 Oct;141:98–112. PMCID: PMC6178871
124. Sun W, Yuill MB. Role of the GABAa and GABAb Receptors of the Central Nucleus of the Amygdala in Compulsive Cocaine-seeking Behavior in Male Rats. Psychopharmacology (Berl). 2020 Dec;237(12):3759–3771. PMCID: PMC7686280
125. Pelloux Y, Minier-Toribio A, Hoots JK, Bossert JM, Shaham Y. Opposite Effects of Basolateral Amygdala Inactivation on Context-Induced Relapse to Cocaine Seeking after Extinction versus Punishment. J Neurosci. 2018 Jan 3;38(1):51–59. PMCID: PMC5761436
126. Madangopal R, Ramsey LA, Weber SJ, Brenner MB, Lennon VA, Drake OR, Komer LE, Tunstall BJ, Bossert JM, Shaham Y, Hope BT. Inactivation of the infralimbic cortex decreases discriminative stimulus-controlled relapse to cocaine seeking in rats. Neuropsychopharmacology. 2021 Oct;46(11):1969–1980. PMCID: PMC8429767
127. Pantazis CB, Aston-Jones G. Lateral septum inhibition reduces motivation for cocaine: reversal by diazepam. Addict Biol. 2019 Mar 21;10.1111/adb.12742. PMCID: PMC6754816
128. Cruz AM, Spencer HF, Kim TH, Jhou TC, Smith RJ. Prelimbic cortical projections to rostromedial tegmental nucleus play a suppressive role in cue-induced reinstatement of cocaine seeking. Neuropsychopharmacology. 2021 Jul;46(8):1399–1406. PMCID: PMC8209220
129. McMurray KMJ, Du X, Brownlee M, Palmer AA. Neuronal overexpression of Glo1 or amygdalar microinjection of methylglyoxal is sufficient to regulate anxiety-like behavior in mice. Behav Brain Res. 2016 Mar 15;301:119–123. PMCID: PMC4728018
130. Harris JJ, Jolivet R, Attwell D. Synaptic Energy Use and Supply. Neuron. 2012 Sep 6;75(5):762–777.
131. Boyer PD. What makes ATP synthase spin? Nature. Nature Publishing Group; 1999 Nov;402(6759):247–249.
132. Du F, Zhu XH, Zhang Y, Friedman M, Zhang N, Uğurbil K, Chen W. Tightly coupled brain activity and cerebral ATP metabolic rate. Proc Natl Acad Sci U S A. 2008 Apr 29;105(17):6409–6414. PMCID: PMC2359810
133. Erecińska M, Silver IA. ATP and Brain Function. J Cereb Blood Flow Metab. SAGE Publications Ltd STM; 1989 Feb 1;9(1):2–19.
134. Swinstead EE, Paakinaho V, Presman DM, Hager GL. Pioneer factors and ATP-dependent chromatin remodeling factors interact dynamically: A new perspective. Bioessays. 2016 Nov;38(11):1150–1157. PMCID: PMC6319265
135. Lepack AE, Werner CT, Stewart AF, Fulton SL, Zhong P, Farrelly LA, Smith ACW, Ramakrishnan A, Lyu Y, Bastle RM, Martin JA, Mitra S, O'Connor RM, Wang ZJ, Molina H, Turecki G, Shen L, Yan Z, Calipari ES, Dietz DM, Kenny PJ, Maze I. Dopaminylation of histone H3 in ventral tegmental area regulates cocaine seeking. Science. 2020 Apr 10;368(6487):197–201. PMCID: PMC7228137
136. Fulton SL, Mitra S, Lepack AE, Martin JA, Stewart AF, Converse J, Hochstetler M, Dietz DM, Maze I. Histone H3 dopaminylation in ventral tegmental area underlies heroin-induced transcriptional and behavioral plasticity in male rats. Neuropsychopharmacology. 2022 Sep;47(10):1776–1783. PMCID: PMC9372029
137. Werner CT, Mitra S, Martin JA, Stewart AF, Lepack AE, Ramakrishnan A, Gobira PH, Wang ZJ, Neve RL, Gancarz AM, Shen L, Maze I, Dietz DM. Ubiquitin-proteasomal regulation of chromatin remodeler INO80 in the nucleus accumbens mediates persistent cocaine craving. Sci Adv. 2019 Oct 9;5(10):eaay0351. PMCID: PMC6785264
138. Werner CT, Mitra S, Auerbach BD, Wang ZJ, Martin JA, Stewart AF, Gobira PH, Iida M, An C, Cobb MM, Caccamise A, Salvi RJ, Neve RL, Gancarz AM, Dietz DM. Neuroadaptations in the dorsal hippocampus underlie cocaine seeking during prolonged abstinence. Proc Natl Acad Sci U S A. 2020 Oct 20;117(42):26460–26469. PMCID: PMC7585028

139. Calipari ES, Godino A, Salery M, Damez-Werno DM, Cahill ME, Werner CT, Gancarz AM, Peck EG, Jlayer Z, Rabkin J, Landry JA, Smith ACW, Defilippi P, Kenny PJ, Hurd YL, Neve RL, Dietz DM, Nestler EJ. Synaptic Microtubule-Associated Protein EB3 and SRC Phosphorylation Mediate Structural and Behavioral Adaptations During Withdrawal From Cocaine Self-Administration. J Neurosci. 2019 Jul 17;39(29):5634–5646. PMCID: PMC6636087
140. Carpenter MD, Hu Q, Bond AM, Lombroso SI, Czarnecki KS, Lim CJ, Song H, Wimmer ME, Pierce RC, Heller EA. Nr4a1 suppresses cocaine-induced behavior via epigenetic regulation of homeostatic target genes. Nat Commun. 2020 Jan 24;11:504. PMCID: PMC6981219
141. Duttke SH, Montilla-Perez P, Chang MW, Li H, Chen H, Carrette LLG, Guglielmo G de, George O, Palmer AA, Benner C, Telese F. Glucocorticoid Receptor-Regulated Enhancers Play a Central Role in the Gene Regulatory Networks Underlying Drug Addiction. Frontiers in Neuroscience [Internet]. 2022 [cited 2022 Jul 22];16. Available from: https://www.frontiersin.org/articles/10.3389/fnins.2022.858427
142. Guglielmo G de, Carrette LL, Kallupi M, Brennan M, Boomhower B, Maturin L, Conlisk D, Sedighim S, Tieu L, Fannon MJ, Martinez A, Velarde N, Kononoff J, Kimbrough A, Simpson S, Smith LC, Shankar K, Crook C, Avelar A, Schweitzer P, Woods LCS, Palmer AA, George O. Characterization of cocaine addiction-like behavior in heterogeneous stock rats [Internet]. bioRxiv; 2021 [cited 2022 Aug 19]. p. 2021.07.22.453410. Available from: https://www.biorxiv.org/content/10.1101/2021.07.22.453410v2
143. Satpathy AT, Granja JM, Yost KE, Qi Y, Meschi F, McDermott GP, Olsen BN, Mumbach MR, Pierce SE, Corces MR, Shah P, Bell JC, Jhutty D, Nemec CM, Wang J, Wang L, Yin Y, Giresi PG, Chang ALS, Zheng GXY, Greenleaf WJ, Chang HY. Massively parallel single-cell chromatin landscapes of human immune cell development and intratumoral T cell exhaustion. Nat Biotechnol. Nature Publishing Group; 2019 Aug;37(8):925–936.
144. Zheng GXY, Terry JM, Belgrader P, Ryvkin P, Bent ZW, Wilson R, Ziraldo SB, Wheeler TD, McDermott GP, Zhu J, Gregory MT, Shuga J, Montesclaros L, Underwood JG, Masquelier DA, Nishimura SY, Schnall-Levin M, Wyatt PW, Hindson CM, Bharadwaj R, Wong A, Ness KD, Beppu LW, Deeg HJ, McFarland C, Loeb KR, Valente WJ, Ericson NG, Stevens EA, Radich JP, Mikkelsen TS, Hindson BJ, Bielas JH. Massively parallel digital transcriptional profiling of single cells. Nat Commun. Nature Publishing Group; 2017 Jan 16;8(1):14049.
145. Navarro Gonzalez J, Zweig AS, Speir ML, Schmelter D, Rosenbloom KR, Raney BJ, Powell CC, Nassar LR, Maulding ND, Lee CM, Lee BT, Hinrichs AS, Fyfe AC, Fernandes JD, Diekhans M, Clawson H, Casper J, Benet-Pagès A, Barber GP, Haussler D, Kuhn RM, Haeussler M, Kent WJ. The UCSC Genome Browser database: 2021 update. Nucleic Acids Research. 2021 Jan 8;49(D1):D1046–D1057.
146. Team TBD. BSgenome.Rnorvegicus.UCSC.rn6: Full genome sequences for Rattus norvegicus (UCSC version rn6). 2014.
147. Kent WJ, Sugnet CW, Furey TS, Roskin KM, Pringle TH, Zahler AM, Haussler and D. The Human Genome Browser at UCSC. Genome Res. 2002 Jun 1;12(6):996–1006.
148. Cunningham F, Allen JE, Allen J, Alvarez-Jarreta J, Amode MR, Armean IM, Austine-Orimoloye O, Azov AG, Barnes I, Bennett R, Berry A, Bhai J, Bignell A, Billis K, Boddu S, Brooks L, Charkhchi M, Cummins C, Da Rin Fioretto L, Davidson C, Dodiya K, Donaldson S, El Houdaigui B, El Naboulsi T, Fatima R, Giron CG, Genez T, Martinez JG, Guijarro-Clarke C, Gymer A, Hardy M, Hollis Z, Hourlier T, Hunt T, Juettemann T, Kaikala V, Kay M, Lavidas I, Le T, Lemos D, Marugán JC, Mohanan S, Mushtaq A, Naven M, Ogeh DN, Parker A, Parton A, Perry M, Piližota I, Prosovetskaia I, Sakthivel MP, Salam AIA, Schmitt BM, Schuilenburg H, Sheppard D, Pérez-Silva JG, Stark W, Steed E, Sutinen K, Sukumaran R, Sumathipala D, Suner MM, Szpak M, Thormann A, Tricomi FF, Urbina-Gómez D,

Veidenberg A, Walsh TA, Walts B, Willhoft N, Winterbottom A, Wass E, Chakiachvili M, Flint B, Frankish A, Giorgetti S, Haggerty L, Hunt SE, IIsley GR, Loveland JE, Martin FJ, Moore B, Mudge JM, Muffato M, Perry E, Ruffier M, Tate J, Thybert D, Trevanion SJ, Dyer S, Harrison PW, Howe KL, Yates AD, Zerbino DR, Flicek P. Ensembl 2022. Nucleic Acids Research. 2022 Jan 7;50(D1):D988–D995.

149. Castro-Mondragon JA, Riudavets-Puig R, Rauluseviciute I, Berhanu Lemma R, Turchi L, Blanc-Mathieu R, Lucas J, Boddie P, Khan A, Manosalva Pérez N, Fornes O, Leung TY, Aguirre A, Hammal F, Schmelter D, Baranasic D, Ballester B, Sandelin A, Lenhard B, Vandepoele K, Wasserman WW, Parcy F, Mathelier A. JASPAR 2022: the 9th release of the open-access database of transcription factor binding profiles. Nucleic Acids Research. 2022 Jan 7;50(D1):D165–D173.
150. Hafemeister C, Satija R. Normalization and variance stabilization of single-cell RNA-seq data using regularized negative binomial regression. bioRxiv. Cold Spring Harbor Laboratory; 2019 Mar 18;576827.
151. Richards LM, Riverin M, Mohanraj S, Ayyadhury S, Croucher DC, Díaz-Mejía JJ, Coutinho FJ, Dirks PB, Pugh TJ. A comparison of data integration methods for single-cell RNA sequencing of cancer samples [Internet]. bioRxiv; 2021 [cited 2022 May 19]. p. 2021.08.04.453579. Available from: https://www.biorxiv.org/content/10.1101/2021.08.04.453579v1
152. Finak G, McDavid A, Yajima M, Deng J, Gersuk V, Shalek AK, Slichter CK, Miller HW, McElrath MJ, Prlic M, Linsley PS, Gottardo R. MAST: a flexible statistical framework for assessing transcriptional changes and characterizing heterogeneity in single-cell RNA sequencing data. Genome Biol [Internet]. 2015 [cited 2020 Oct 26];16. Available from: https://www.ncbi.nlm.nih.gov/pmc/articles/PMC4676162/ PMCID: PMC4676162
153. Wu T, Hu E, Xu S, Chen M, Guo P, Dai Z, Feng T, Zhou L, Tang W, Zhan L, Fu X, Liu S, Bo X, Yu G. clusterProfiler 4.0: A universal enrichment tool for interpreting omics data. The Innovation. 2021 Aug 28;2(3):100141.
154. Stuart T, Srivastava A, Lareau C, Satija R. Multimodal single-cell chromatin analysis with Signac. bioRxiv. Cold Spring Harbor Laboratory; 2020 Nov 10;2020.11.09.373613.
155. Quinlan AR, Hall IM. BEDTools: a flexible suite of utilities for comparing genomic features. Bioinformatics. 2010 Mar 15;26(6):841–842.
156. Cusanovich DA, Daza R, Adey A, Pliner H, Christiansen L, Gunderson KL, Steemers FJ, Trapnell C, Shendure J. Multiplex Single Cell Profiling of Chromatin Accessibility by Combinatorial Cellular Indexing. Science. 2015 May 22;348(6237):910–914. PMCID: PMC4836442
157. Deerwester S, Dumais ST, Furnas GW, Landauer TK, Harshman R. Indexing by latent semantic analysis. Journal of the American Society for Information Science. 1990;41(6):391–407.
158. Korsunsky I, Millard N, Fan J, Slowikowski K, Zhang F, Wei K, Baglaenko Y, Brenner M, Loh P ru, Raychaudhuri S. Fast, sensitive and accurate integration of single-cell data with Harmony. Nature Methods. Nature Publishing Group; 2019 Dec;16(12):1289–1296.
159. Yirga AA, Melesse SF, Mwambi HG, Ayele DG. Negative binomial mixed models for analyzing longitudinal CD4 count data. Sci Rep. Nature Publishing Group; 2020 Oct 7;10(1):16742.
160. Purcell S, Neale B, Todd-Brown K, Thomas L, Ferreira MAR, Bender D, Maller J, Sklar P, de Bakker PIW, Daly MJ, Sham PC. PLINK: A Tool Set for Whole-Genome Association and Population-Based Linkage Analyses. Am J Hum Genet. 2007 Sep;81(3):559–575. PMCID: PMC1950838
161. Heinz S, Benner C, Spann N, Bertolino E, Lin YC, Laslo P, Cheng JX, Murre C, Singh H, Glass CK. Simple combinations of lineage-determining transcription factors prime cis-regulatory elements required for macrophage and B cell identities. Mol Cell. 2010 May

28;38(4):576–589. PMCID: PMC2898526

Figure Legends

Figure 1

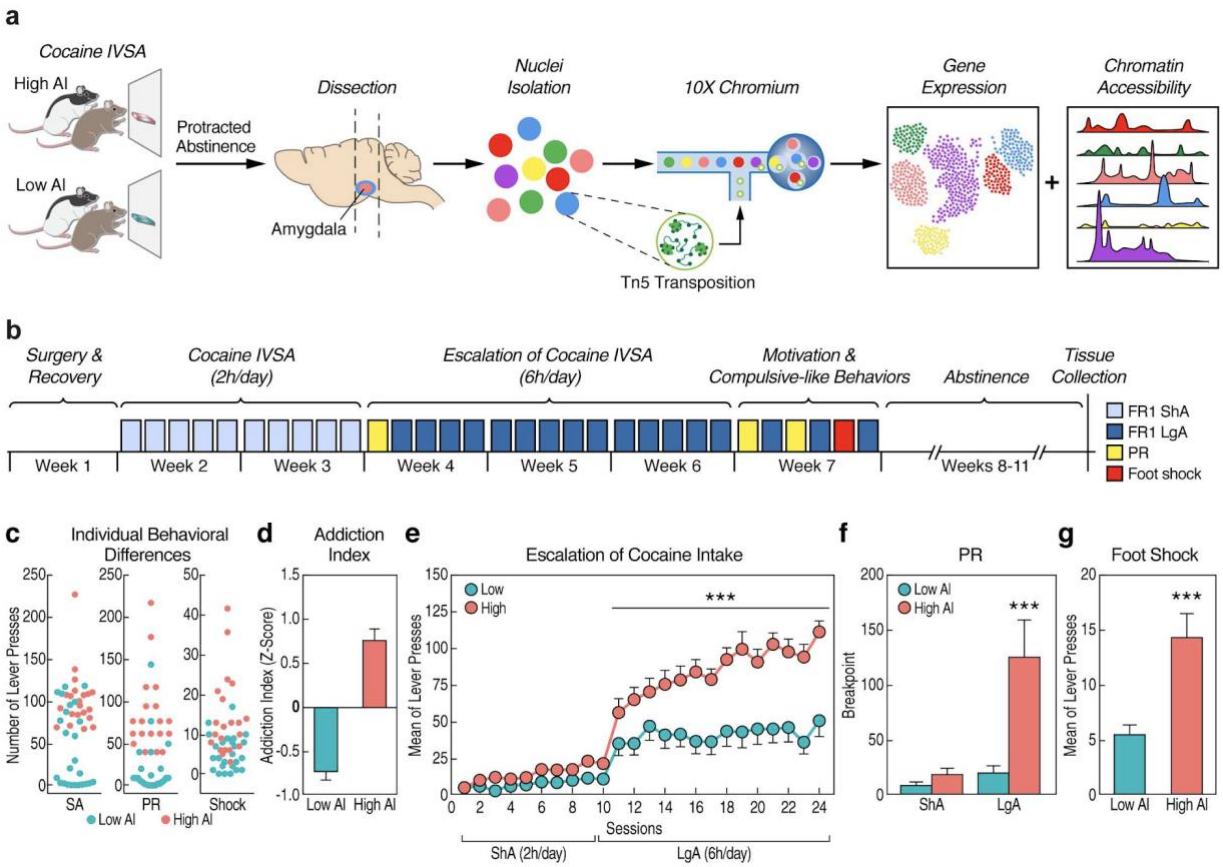

Figure 1. Experimental design and rat IVSA cocaine model of addiction. a) Schematic of the study design. **b)** Timeline of the behavioral protocol. **c)** Individual differences in total number of lever presses in self-administration (SA), progressive ratio (PR) and shock-paired (Shock) sessions for each rat. **d)** Mean addiction index scores in high and low AI rats. **e)** Mean number of lever presses across each ShA and LgA IVSA session in high (n=21) and low (n=25) AI rats (*** $p < 0.001$, two-way repeated measures ANOVA interaction time x group $F_{13,572}=4.175$). **f)** Breakpoint analysis of high (n=21) and low (n=25) AI rats under ShA versus LgA (*** $p<0.001$ mixed effect model, addiction index × phase interaction, $p=0.0049$, $F_{1,41}=8.83$). **g)** Mean number of lever presses when paired with electric footshock in high (n=21) and low AI (n=25) rats (***$p<0.001$, unpaired Student's t-test, $t_{44}=3.936$). Error bars in panels d-g represent the standard error of the mean.

Figure 2

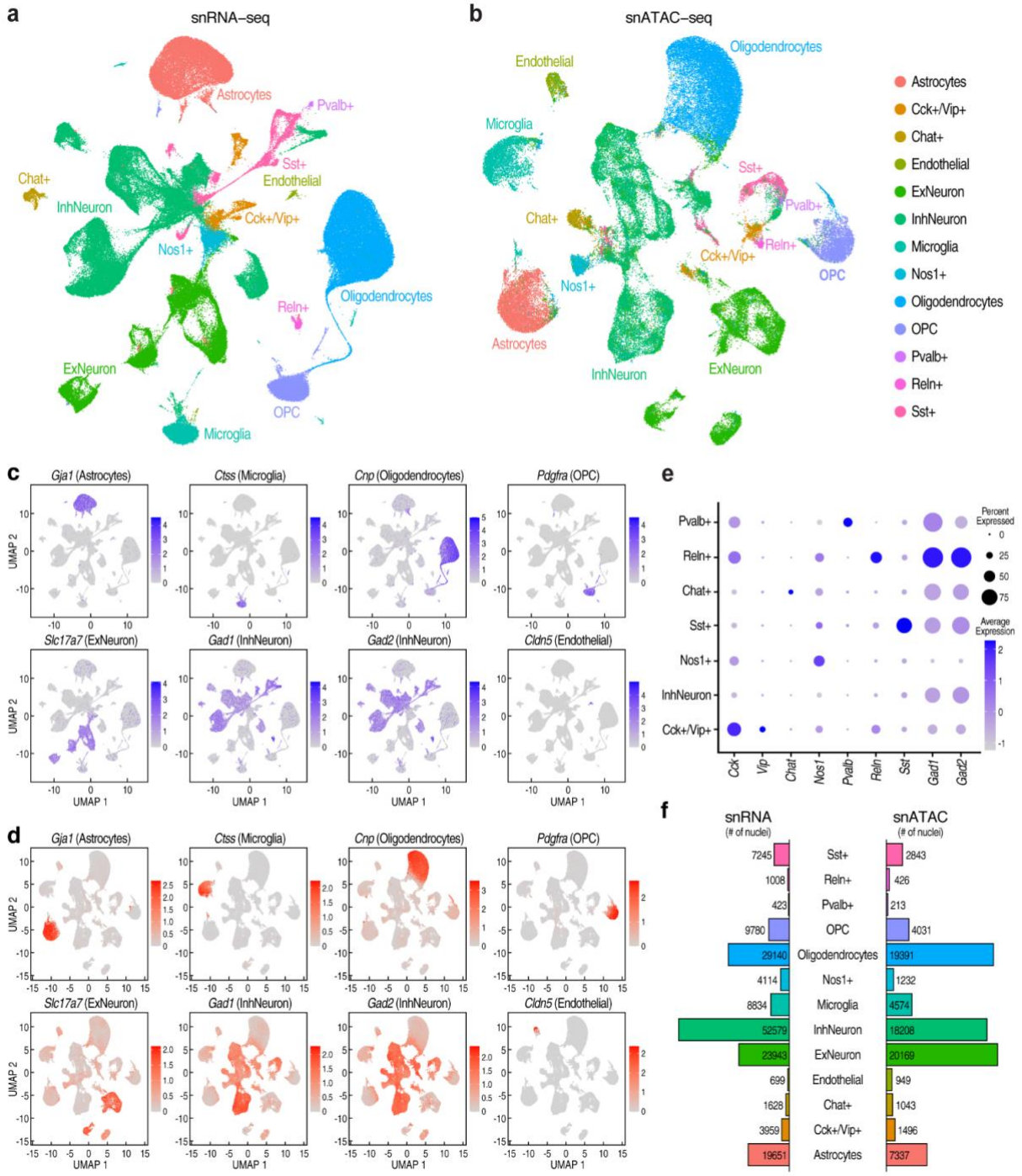

Figure 2. Summary of single nucleus RNA-seq and ATAC-seq data from the rat amygdala. a) Uniform Manifold Approximation And Projection (UMAP) plot of single nucleus RNA-seq (snRNA-seq) data from the rat amygdala. Data are combined across 19 samples, with high, low, and naive addiction index labels. Cells are colored by cluster assignments

performed with K-nearest neighbors. We assigned cell type labels to the clusters based on the expression of known marker genes. **b)** UMAP plot of single nucleus ATAC-seq data from 12 rat amygdala samples. snATAC-seq data was integrated with the snRNA-seq data and cluster labels were transferred to the snATAC-seq cells. **c)** Feature plot showing expression of marker genes used to label major subsets of cells: *Gja1* (astrocytes), *Ctss* (microglia), Cnp (oligodendrocytes), *Pdgfra* (oligodendrocyte precursor cells (OPCs), *Slc17a7* (excitatory neurons), *Gad1* and *Gad2* (inhibitory neurons), and *Cldn5* (endothelial cells). **d)** Feature plot showing imputed gene expression of cell type-specific marker genes in snATAC-seq dataset. **e)** Expression of marker genes in cell clusters corresponding to highly specific subsets of inhibitory neurons. The shading and diameter of each circle indicate the estimated mean expression and the percentage of cells within the cluster in which the marker gene was detected. **f)** The number of nuclei assigned to each cell type cluster for the snATAC-seq and snRNA-seq datasets.

Figure 3

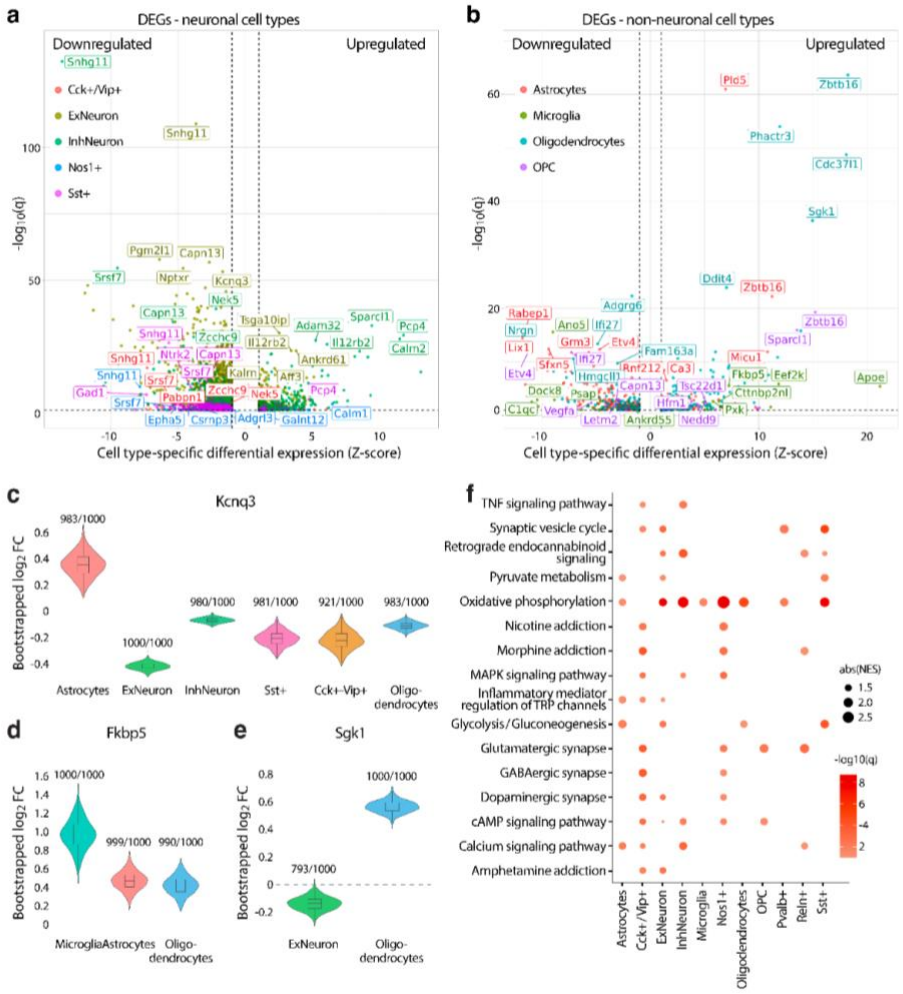
a
DEGs - neuronal cell types
Downregulated
Upregulated
Cck+/Vip+
ExNeuron
InhNeuron
Nos1+
Sst+
-log10(q)
Cell type-specific differential expression (Z-score)
b
DEGs - non-neuronal cell types
Downregulated
Upregulated
Astrocytes
Microglia
Oligodendrocytes
OPC
-log10(q)
Cell type-specific differential expression (Z-score)
c
Kcnq3
Bootstrapped log2 FC
983/1000
1000/1000
980/1000
981/1000
921/1000
983/1000
Astrocytes
ExNeuron
InhNeuron
Sst+
Cck+-Vip+
Oligo-dendrocytes
d
Fkbp5
Bootstrapped log2 FC
1000/1000
999/1000
990/1000
Microglia
Astrocytes
Oligo-dendrocytes
e
Sgk1
Bootstrapped log2 FC
1000/1000
793/1000
ExNeuron
Oligo-dendrocytes
f
TNF signaling pathway
Synaptic vesicle cycle
Retrograde endocannabinoid signaling
Pyruvate metabolism
Oxidative phosphorylation
Nicotine addiction
Morphine addiction
MAPK signaling pathway
Inflammatory mediator regulation of TRP channels
Glycolysis/Gluconeogenesis
Glutamatergic synapse
GABAergic synapse
Dopaminergic synapse
cAMP signaling pathway
Calcium signaling pathway
Amphetamine addiction
abs(NES)
-log10(q)
Astrocytes
Cck+/Vip+
ExNeuron
InhNeuron
Microglia
Nos1+
Oligodendrocytes
OPC
Pvalb+
Reln+
Sst+

Figure 3. Differential gene expression between high and low addiction index rats. a) Volcano plot summarizing differential gene expression between high and low AI rats. Points are colored by cell type, and the five most significant (FDR<10%) up- and downregulated genes in each cell type are indicated with labels. Within each cell type, we normalized the log fold changes reported by Seurat with a z-score and plotted the cell type-specific z-scores of the log fold changes on the x-axis (positive fold change = higher expression in high AI rats; negative fold change = higher expression in low AI rats). The $-\log_{10}$ false discovery rate (FDR) corrected p-values (q-values) are plotted on the y-axis. **b)** Volcano plot summarizing differential gene expression between high and low AI rats for non-neuronal (glial) cell type clusters. **c-e)** Violin plots showing distribution of $\log_2$FC from the negative binomial test performed in 1000 bootstrap iterations. Fractions indicate the number of bootstrap iterations in which the log2FC estimate was significantly different than 0. Bootstrap distributions were obtained for cell types in which the following genes had significant differential expression (FDR<10%): **c)** *Kcnq3*; **d)** *Fkbp5*; **e)** *Sgk1*. **f)** KEGG pathways that are enriched for differentially expressed genes by cell type. Size of dot indicates -log10(q) while color indicates normalized enrichment score (NES), which is a metric of GSEA. Only pathways/cell types where q<0.1 are visualized.

Figure 4

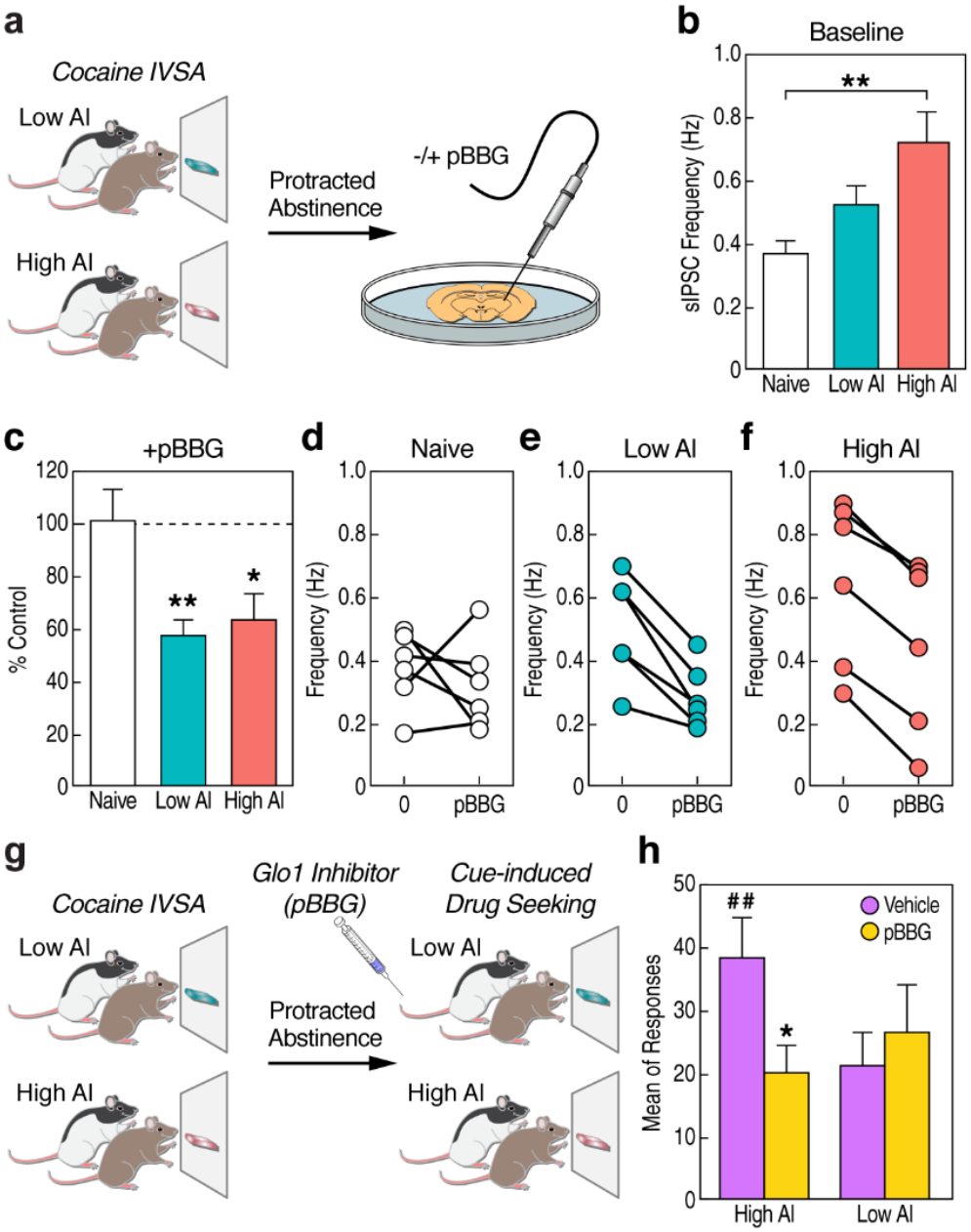

Figure 4. Electrophysiology and GLO1 inhibition experiments implicate GABAergic inhibition in cocaine addiction-like behaviors. a) Schematic showing animal model used for electrophysiology recording in CeA slices from HS rats subjected to 4 weeks of abstinence from cocaine IVSA. Electrophysiological recordings were taken before and after pBBG (S-bromobenzylglutathione cyclopentyl diester) treatment. **b)** Baseline iPSC frequency (measured before pBBG injection). Significant differences in the means between the three groups were observed (**$p < 0.01$; one-way ANOVA $F_{2,22}=6.77$, followed by post-hoc

comparison using Tukey's HSD). **c)** sIPSC frequency following pBBG treatment. We observed reduced frequency in the CeA slices from high and low AI rats following pBBG treatment (**$p < 0.01$, *$p<0.05$ following Bonferroni correction; unpaired two-sided Student's t-test). Change in sIPSC frequency following pBBG treatment in **d)** naive, **e)** low**,** and **f)** high rats**. g)** Schematic of animal model used to test cocaine-seeking behavior. Rats were injected with pBBG following a period of prolonged abstinence and re-exposed to the self-administration chambers in the absence of cocaine. **h)** Following injection of pBBG, high AI rats (n=12) showed significantly higher cocaine-seeking behavior compared to low AI rats (n=14), which was reduced by pBBG treatment (## $p<0.001$, *$p<0.05$ following Bonferroni correction; two-way ANOVA for each measure). Error bars in panels b,c, and h represent the standard error of the mean.

Figure 5

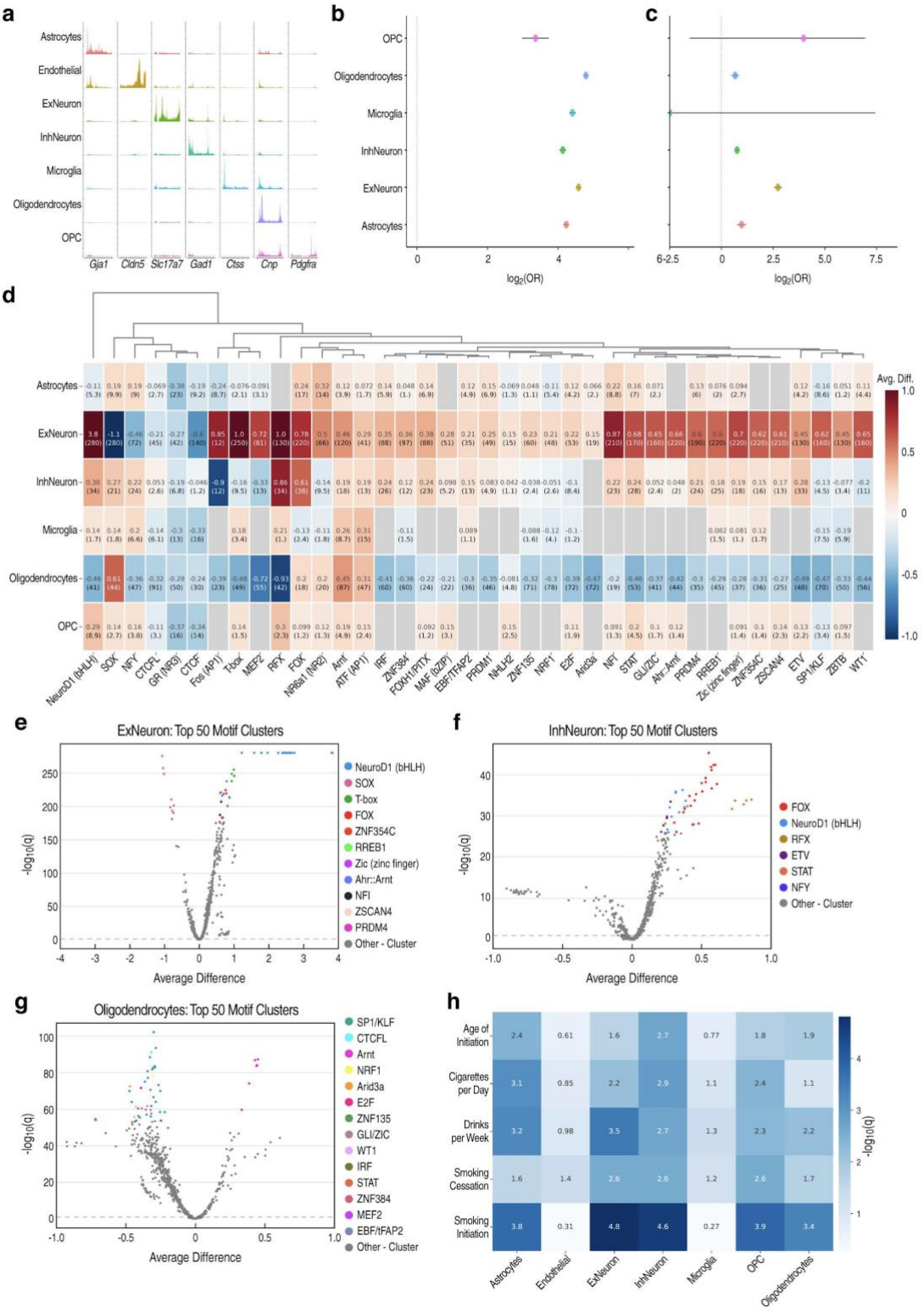
a
Astrocytes
Endothelial
ExNeuron
InhNeuron
Microglia
Oligodendrocytes
OPC
Gja1
Cldn5
Slc17a7
Gad1
Ctss
Cnp
Pdgfra
b
OPC
Oligodendrocytes
Microglia
InhNeuron
ExNeuron
Astrocytes
log2(OR)
c
log2(OR)
d
Avg. Diff.
Astrocytes
ExNeuron
InhNeuron
Microglia
Oligodendrocytes
OPC
NeuroD1 (bHLH)
SOX
NFY
CTCFL
GR (NR3)
CTCF
Fos (AP1)
T-box
MEF2
RFX
FOX
NR6a1 (NR2)
Arnt
ATF (AP1)
IRF
ZNF384
FOXH1/PITX
MAF (bZIP)
EBF/TFAP2
PRDM1
NHLH2
ZNF135
NRF1
E2F
Arid3a
NFI
STAT
GLI/ZIC
Ahr::Arnt
PRDM4
RREB1
Zic (zinc finger)
ZNF354C
ZSCAN4
ETV
SP1/KLF
ZBTB
WT1
e
ExNeuron: Top 50 Motif Clusters
-log10(q)
Average Difference
NeuroD1 (bHLH)
SOX
T-box
FOX
ZNF354C
RREB1
Zic (zinc finger)
Ahr::Arnt
NFI
ZSCAN4
PRDM4
Other - Cluster
f
InhNeuron: Top 50 Motif Clusters
-log10(q)
Average Difference
FOX
NeuroD1 (bHLH)
RFX
ETV
STAT
NFY
Other - Cluster
g
Oligodendrocytes: Top 50 Motif Clusters
-log10(q)
Average Difference
SP1/KLF
CTCFL
Arnt
NRF1
Arid3a
E2F
ZNF135
GLI/ZIC
WT1
IRF
STAT
ZNF384
MEF2
EBF/tFAP2
Other - Cluster
h
Age of Initiation
Cigarettes per Day
Drinks per Week
Smoking Cessation
Smoking Initiation
Astrocytes
Endothelial
ExNeuron
InhNeuron
Microglia
OPC
Oligodendrocytes
-log10(q)

Figure 5. Analysis of chromatin accessibility and regulatory elements involved in cocaine dependence. a) Pseudobulk chromatin accessibility at the promoter regions of marker genes for major cell types identified in our analysis. **b)** Significant DEGs (FDR<10%) for each major cell type are enriched for promoters with differentially accessible chromatin accessibility (FDR<10%; Fisher's exact test) in the snATAC-seq data. This indicates that the snRNA-seq and snATAC-seq results are consistent and indicate that long-term transcriptional changes are associated with changes in chromatin accessibility of gene promoters. **c)** Cell type-specific differentially accessible peaks (FDR<10%; Fisher's exact test) are enriched in TSS/promoter regions compared to non-TSS/promoter regions. Error bars in b,c represent 95% confidence intervals for log2 odds ratios (ORs). **d)** Heatmap showing differential activity of various motifs in the significant differential peaks of each cell type. Values indicate average difference of chromVar deviation scores with -log10(p) in parentheses below. There are many cases where motifs display increased activity in the peaks which are more accessible in upregulated peaks in neurons while also displaying decreased activity in downregulated peaks in oligodendrocytes. **e-g)** Volcano plots showing average difference (x-axis) and -log10(q) (y-axis) of chromVAR deviation scores for top 50 motif clusters in **e)** excitatory neurons, **f)** inhibitory neurons, and **g)** oligodendrocytes. **h)** LD score regression results showing significance (-log10p) of enrichment of heritability for several traits related to alcohol and nicotine addiction in cell type-specific accessible chromatin regions (mapped to hg19).